A general stability analysis of structural systems subjected to circulatory loading or thermal radiation in the elastic and elasto-plastic range

Arif, Ghazi Majid

1991

LUND UNIVERSITY · SWEDEN
INSTITUTE OF TECHNOLOGY
DEPARTMENT OF FIRE SAFETY ENGINEERING
CODEN: SE–LUTVDG/TVBB–3060
ISSN 0284–933X

GHAZI MAJID ARIF

A GENERAL STABILITY ANALYSIS OF STRUCTURAL SYSTEMS SUBJECTED TO CIRCULATORY LOADING OR THERMAL RADIATION IN THE ELASTIC AND ELASTO-PLASTIC RANGE

Lund, August, 1991

ABSTRACT

The paper examines the nonlinear behaviour of one– and two–degree–of–freedom discrete mechanical models subjected to partial follower load under conditions at which divergence instability occurs. Section (1.6) of the paper deals with the dynamic instability of an elastoplastic damped strut compressed by partial follower force at the free end. Space–time curves for the system are presented and discussed. The paper treats as well the static instability and response of continuous cantilever columns with eccentric follower forces and with various types of initial curvatures. Finally, instability and response of a satellite boom subjected to thermal radiation and partial follower force is dealt with.

1.1 GENERAL INTRODUCTION

In the last three decades great attention has been devoted to nonconservative systems in which stability is lost either by flutter in one range of a parameter or by divergence in another. The study of such systems can be traced back to the work of Nikolai in the late nineteen twenties. He adopted the kinetic stability criterion as he arrived at a paradoxical conclusion in his stability analysis of a compressed and twisted bar.

Nonconservative systems can be found in the following groups:

1. Elastic systems subjected to deflection dependent forces
2. whirling of rotating shafts
3. wandering of driven or jacked piles in the ground
4. stability of pipes conveying fluids and elastic bodies in gas flow
5. thermal flutter.

The simplest example belonging to group 1 is the Beck's rod. Aircraft wings acted upon by the thrust of a jet engine can be idealized by a cantilever rod subjected to a transverse non–conservative end force.

Flexible shafts with a controlled speed of revolution are nonconservative systems. for details see Reference [1]. The deviation of the pile heads during driving or jacking in the ground from the assumed line of action of up to 2 m has been reported by York [2]. Burgess [3] pointed out the directional instability of jacked or driven piles and of the nonconservative nature of some of the forces involved. This is attributed to the path dependent shear force developed along the pile as successive portions of it interact with the soil mass. Eccentricity and initial curvature influence the directional deviation of the driven piles [4].

Group 4 comprises a wide range of applications to structural systems. As an example, the dynamic instability (flutter), which has plagued aircraft designs for a long time, belongs to this group. For further details, see for example Reference [5].

Flow induced instabilities of pipes or cylindrical structures subjected to either internal or external flows can be found in many engineering designs. Simplified models of Becks rod have been treated in the literature extensively [6] and was

denounced by Sugiyama et al [7]. In most of the studies, the influence of eccentricity and nonlinearity has been ignored. The post–buckling analysis of conservative systems by Koiter [8] by a static perturbation technique [9], has been extended by Thompson and Hunt [10] to discrete systems, covering bifurcation points and limit points. Other studies on the line of Koiter are due to Hunt, Sewell and Huseyin [11]. Post buckling analysis of symmetric nonconservative systems on Thompson's line of works was initiated by Burgess and Levinson [12] and they considered soft flutter.

Plaut in a number of papers [13, 14, 15] considered the post–buckling and branching out behaviour of discrete and continuous systems.

Nonlinear discrete and nonconservative systems was investigated for the critical case by Hagedorn [16], making use of a procedure by Salvadori. Nonlinear analysis of nonconservative elastic systems involving Hopf bifurcation was carried out by Sethna and Shapiro [17] adopting the method of Hopf and the method of integral manifolds.

The recent rediscovery of Poincaré maps or chaos maps in nonlinear mechanics has been a great temptation and impulse to new works on nonconservative nonlinear systems, see Guckenheimer and Holmes [18]. Centre manifold theory has been used to study the flutter and divergence bifurcation of a double pendulum by Scheidl et al [19] and Jin and Matsuzaki [20]. Chaos like phenomena were found by Kounadis [21] in his study on nonconservative precritical deformations. A modification of the perturbation technique used in the analysis by Mandadi and Huseyin [22] of gradient systems is used in the nonlinear bifurcation analysis of nongradient systems. The method leads to asymptotic results.

The first study of stability of pipes conveying fluids belonging to group 4 is due to Bourrières 1939, [23]. Flow in articulated pipes has been successfully modelled in the laboratory by Gregory and Paidoussis [24] and Benjamin [25].

Other axial moving materials encompasses high speed magnetic and paper tapes, band saws, conveyer belts, aerial cable tramways [26]. Another type of nonconservative systems is flexible antennas (booms) attached to artificial satellites subjected to thermal radiation [27].

Stability of nonconservative systems in the elastoplastic range was first investigated by Augusti [28]. Chernukha in a number of articles studied the Rider–Zieglers model of cantilever columns subjected to follower forces [29, 30].

The linear and nonlinear analysis of the stability of structural frame works subjected to compressive follower forces at a joint has been studied by Kounadis et al [31, 32, 33]. The stability of arches with circulatory loading has been analysed by Argyris and Symeonidis in the pre and post flutter region [34, 35]. Oran and Reagan [36] investigated the problem of buckling of a cantilever arch subjected to configurations dependent loads. Another work on the buckling and post–buckling of arches subjected to follower forces is due to Hasegawa et al [37].

On the experimental side, the nonconservative forces are difficult to produce in the laboratory. Bolotin suggested for instance, the simulation of such forces by the reaction of a jet. For details of the experimental studies of columns compressed by follower forces, see Reference [38].

This report concerns itself with the investigation of stability of nonconservative systems taking into account the influence of eccentricity and initial deflections. The theoretical findings are substantiated by experimental studies whenever possible.

1.2 BUCKLING AND POST BUCKLING OF SIMPLE MECHANICAL SYSTEMS

The post–buckling response and the actual load–carring capacity of structural systems arose from the necessity to explain the wide scatter between the theoretical and experimental buckling results, especially in shell buckling problems as documented by Lundquist [9] and Donnel [40].

As the initial imperfections are random quantities and in most column buckling problems, the following types of imperfections are present:

1. load conditions causing disuniformities

2. initial curvature of load eccentricity due to geometric character of the column
3. residual stresses and variations in the yield point of the particular column

Augusti in his doctoral thesis presented a number of mechanical one–degree–of–freedom models and investigated the influence of initial deflection on the stability of the models, using nonlinear large displacement analysis. In the following sections, a number of mechanical models (discrete and continuous) will be analysed in the elastic and in the elastoplastic range for instability.

1.3 BUCKLING AND POST BUCKLING OF ONE–DEGREE–OF–FREEDOM MECHANICAL MODEL

A simple one–degree–of–freedom model comprising an infinitely rigid cantilever with an elastic hinge at the bottom and compressed by an eccentric follower force at the top is shown in Figure 1. The initial out–of–plumb of the upright rotation is denoted by ϕ_o and the total upright rotation by ϕ. The expression for the moment about the hinge is given by

$$M = Pe\ \cos(\phi - \phi_p) + P \cdot L\ \sin(\phi - \phi_p) \tag{1.3.1}$$

where $\phi_p = k\phi + \bar{k}\ \sin\ \phi$

and $M = c(\phi - \phi_o)$ (1.3.2)

Introducing the following nondimensional quantities $\epsilon = e/L$, $\beta = PL/c$ then equations (1.3.1) and (1.3.2) can be written as

$$\beta = \frac{\phi - \phi_o}{\epsilon\cos(\gamma\phi - \bar{k}\sin\phi) + \sin(\gamma\phi - \bar{k}\sin\phi)} \tag{1.3.3}$$

where $\gamma = 1 - k$ (1.3.3.a)

for various values of ϕ_o and ϵ. The values of β were found with values of ϕ fixed between $-\pi/2$ and $\pi/2$. In Figure 2 the influence of eccentricity ϵ on the loading β is shown for five values of γ. It is evident from the figure that the

loading increases with the decrease of γ and the increase of the eccentricity parameter ϵ.

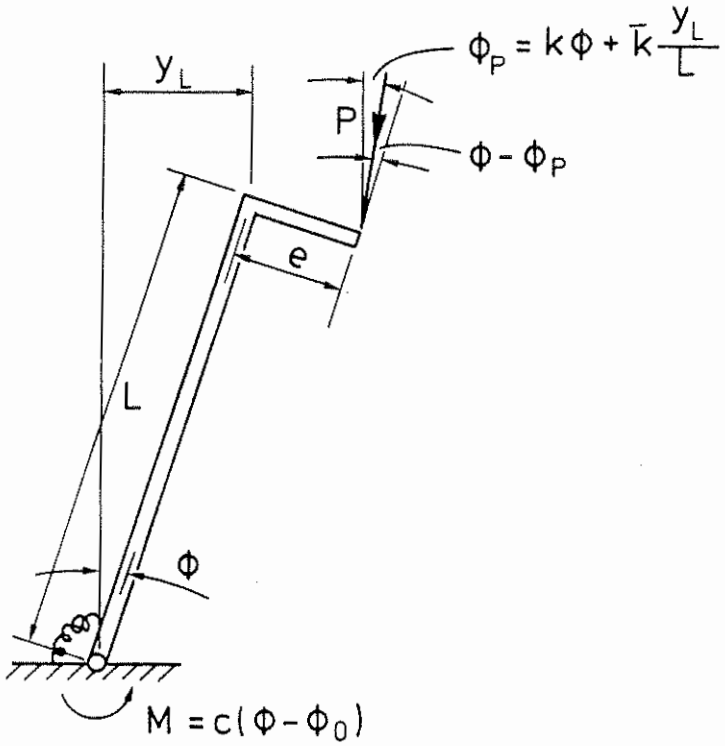

Fig. 1 One–degree–of–freedom mechanical model

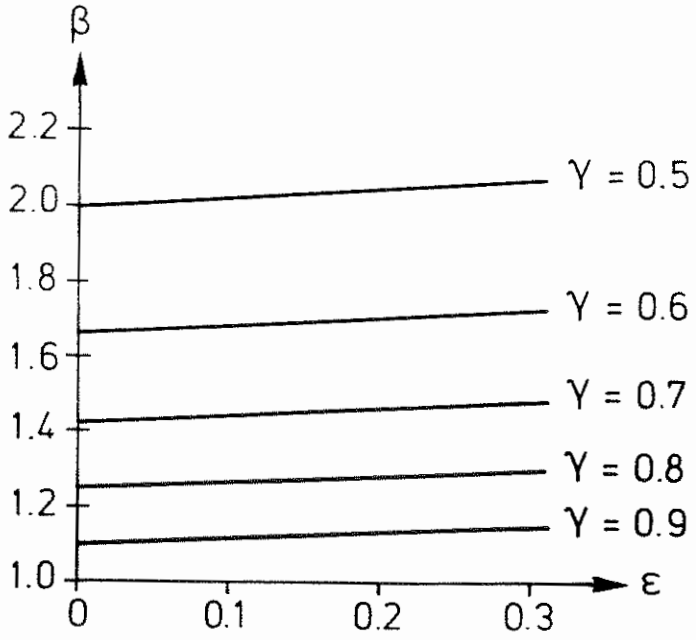

Fig.2 Loading β versus eccentricity ϵ for various values of the parameter γ. $\bar{k} = 0$

In Figure 3, the load–deformation relationship according to equation (1.3.3) is plotted for values of ϕ between $-\pi/2$ and $\pi/2$ for k = 0.8 and $\bar{k}$ = 0. The collapse load β_c for the case with eccentricity ϵ = 0.01 is given at the point at which a horizontal tangent touches the curve (β_c = 5.25). Analytically the abscissa ϕ_c of the collapse point can be found from equating to zero the derivative $d\beta/d\phi$ obtained from equation (1.3.3).

In Figure 4, the load–deflection curves have been plotted for six values of ϕ_o with γ = 0.5 and $\bar{k}$ = ϵ = 0.0. It can be seen from the figure that two separate equilibrium paths exist. The first path belongs to the gradual loading from the initial point ($\phi_o > 0$) and the second secondary path for $\phi_o < 0$ in which the column is moved by some external disturbance.

Finally, Figure 5 depicts load–deformation curves for six values of the nonconservative parameter γ with ϕ_o = 0.1 and $\bar{k}$ = ϵ = 0.0 and portrays two separate equilibrium paths.

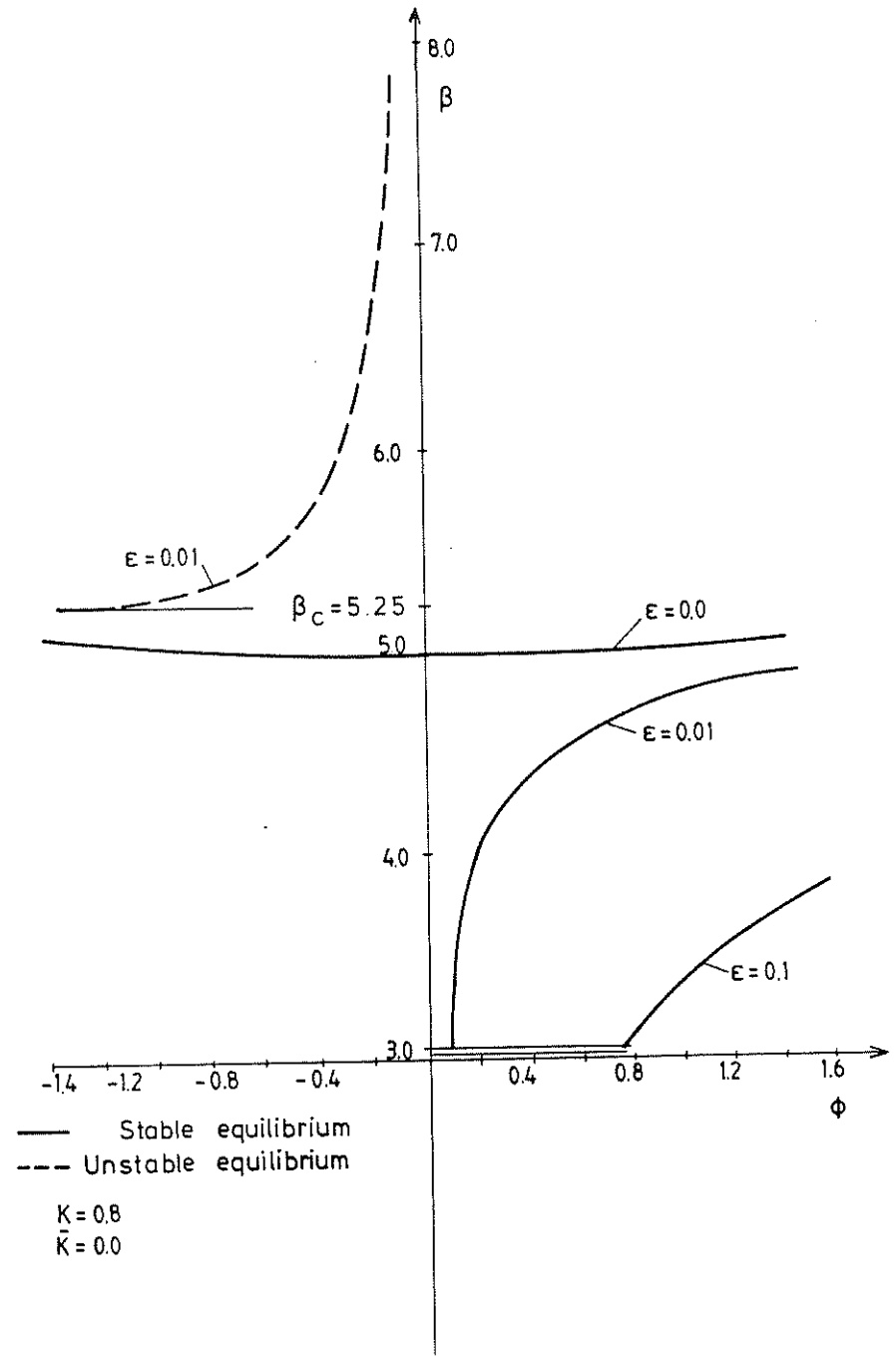

Fig. 3 Loading β versus angle ϕ for three values of eccentricity parameter ϵ

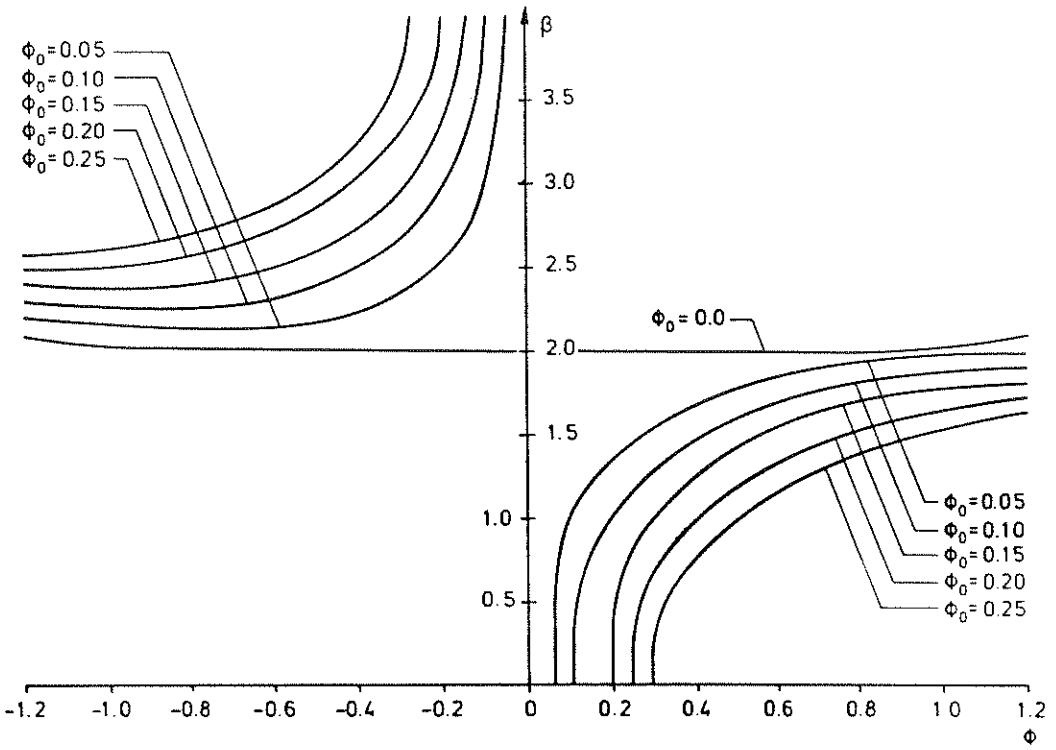

Fig. 4 Deflection–load curves with $\gamma = 0.5$ and $\epsilon = \bar{k} = 0.0$

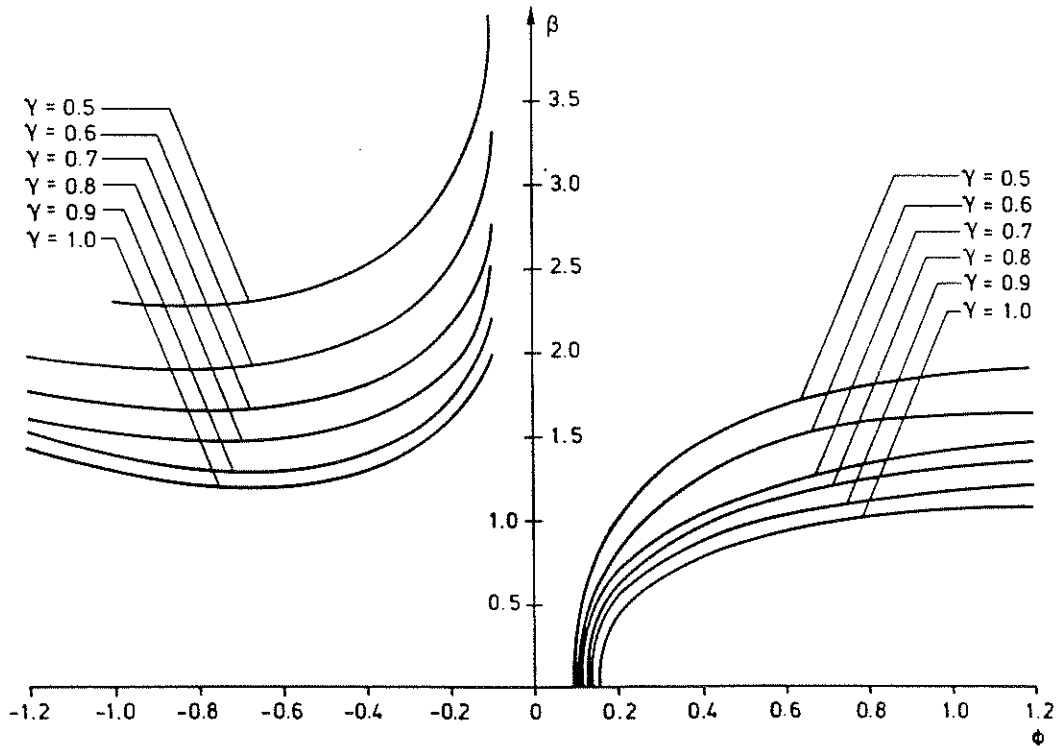

Fig. 5 Deflection–load curves with $\phi_0 = 0.1$, $\epsilon = 0.0$ and $\bar{k} = 0.0$

1.4 TWO–DEGREE–OF–FREEDOM MODEL

The model considered in this section is depicted in Figure 6. It consists of a double pendulum acted upon by an eccentric partial follower force at the top.

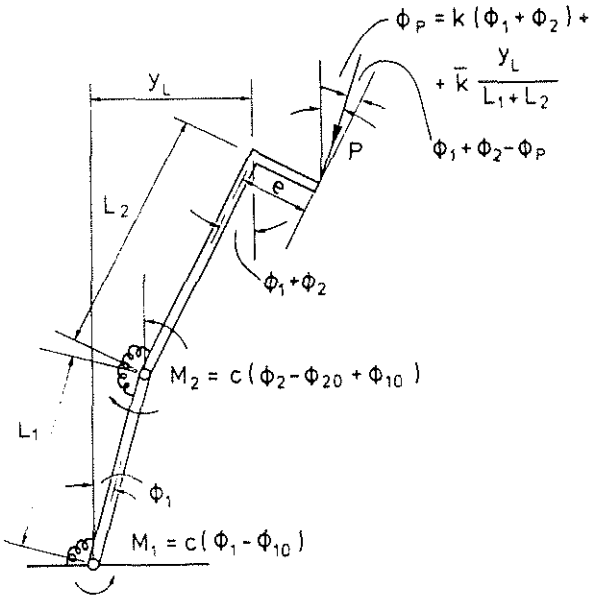

Fig.6 Two–degree–of–freedom model

The expressions for the moments at the hinges are given by

$$M_1 = PL_1 \sin(\phi_1 - \phi_p) + PL_2 \sin(\phi_1 + \phi_2 - \phi_p) + Pe \cos(\phi_1 + \phi_2 - \phi_p)$$

$$M_2 = PL_2 \sin(\phi_1 + \phi_2 - \phi_p) + Pe \cos(\phi_1 + \phi_2 - \phi_p) \qquad (1.4.1)$$

where

$$\sin(\phi_1 - \phi_p) = \sin\left\{-\phi_2 + \gamma\,\phi - \frac{\bar{k}}{1+\alpha}[\sin(\phi - \phi_2) + \alpha\sin\phi]\right\}$$

$$M_1 = c(\phi - \phi_2 - R - \phi_{20})$$
$$M_2 = c(\phi_2 + R)$$

and $\phi = \phi_1 + \phi_2$
$R = -\phi_{20} + \phi_{10}$
$\alpha = L_2/L_1, \quad \gamma = 1 - k \qquad (1.4.2)$

Substituting (1.4.2) into (1.4.1), the dimensionless load β is given as

$$\beta = \frac{\phi_2 + R}{\alpha \sin(\phi - \phi_p) + \epsilon \cos(\phi - \phi_p)} \tag{1.4.3}$$

with

$$\beta = PL_1/c \quad \text{and} \quad \epsilon = e/L_1 \tag{1.4.4}$$

Substituting for β in equation (1.4.1), the following expression is obtained

$$(\phi - \phi_{20}) = \frac{(\phi_2 + R)\,\Delta}{\alpha\sin(\phi - \phi_p) + \epsilon \cos(\phi - \phi_p)} \tag{1.4.5}$$

where

$$\Delta = \sin(\phi_1 - \phi_p) + 2\alpha \sin(\phi - \phi_p) + 2\epsilon \cos(\phi - \phi_p) \tag{1.4.6}$$

By assigning values between π and $-\pi$ to ϕ, the value of ϕ_2 will be found from equation (1.4.5) and the load β will be given by equation (1.4.3). A Nag Library Subroutine has been used to find the values of ϕ_2 from expression (1.4.5).

For $\bar{k} = 0$, $\alpha = 1.0$, $\phi_{20} = \phi_{10} = 0$, equation (1.4.4) becomes

$$\phi = \frac{\phi_2 \Delta_1}{\sin\gamma\ \phi + \epsilon \cos\gamma\phi} \tag{1.4.7}$$

where

$$\Delta_1 = \sin(\gamma\ \phi - \phi_2) + 2\sin\gamma\ \phi + 2\epsilon \cos\gamma\ \phi \tag{1.4.8}$$

Equation (1.4.3) may be written differently by introducing the following dimensionless quantities

$$\bar{\beta} = \frac{P(L_1+L_2)}{c}, \quad \bar{\epsilon} = \frac{e}{L_1+L_2} \tag{1.4.9}$$

Then the new expression for the loading is given by

$$\bar{\beta} = \frac{\phi_2 + R}{\frac{\alpha}{1+\alpha} \sin(\phi-\phi_p)+\bar{\epsilon}\cos(\phi-\phi_p)} \tag{1.4.10}$$

Subsequently, equations (1.4.5) and (1.4.6) may be rewritten as

$$\phi - \phi_{20} = \frac{(\phi_2 + R)\bar{\Delta}}{\frac{\alpha}{1+\alpha} \sin(\phi-\phi_p) + \bar{\epsilon}\cos(\phi-\phi_p)} \tag{1.4.11}$$

and

$$\bar{\Delta} = \frac{1}{1+\alpha} \sin(\phi_1 - \phi_p) + \frac{2\alpha}{1+\alpha} \sin(\phi-\phi_p) + 2\bar{\epsilon} \cos(\phi-\phi_p) \tag{1.4.12}$$

Both versions of the load–deflection equations were used in the numerical calculations.

In Figure 7, the loading β (from equation (1.4.3)) is plotted versus ϕ_1 for $k = 5/9$ and $\alpha = 1.0$ ($\phi_{10} = \phi_{20} = 0.001$, $\epsilon = \bar{k} = 0$). The critical buckling load for the perfect system, from a linear analysis, is 1.5. The corresponding configuration at various loadings shown in Figure 8. The linear dynamic analysis has been studied thoroughly by Pettersson [41].

Figures 9 and 10 show the configurations of the pendulum under various loadings (equations (1.4.10) and (1.4.11)) for two values of γ. Finally Figure 11 depicts the load β versus the torsional angle ϕ_1 for five values of γ. The initial deflections are $\phi_{10} = \phi_{20} = 0.001$ and the load eccentricity is $\bar{\epsilon} = 0.2$.

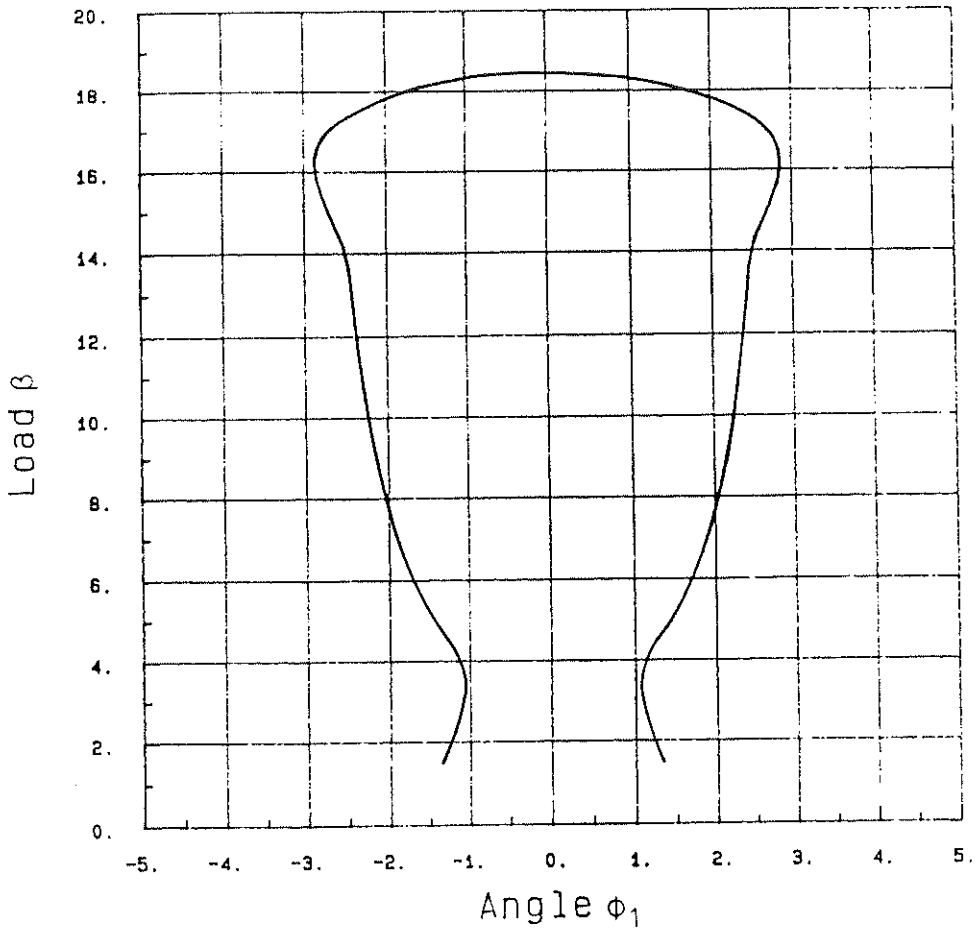

Fig. 7 Loading β versus angle ϕ_1 for $\gamma = 4/9$, $\alpha = 1.0$, $\bar{k} = 0.0$, $\epsilon = 0.0$, $\phi_{10} = \phi_{20} = 0.001$

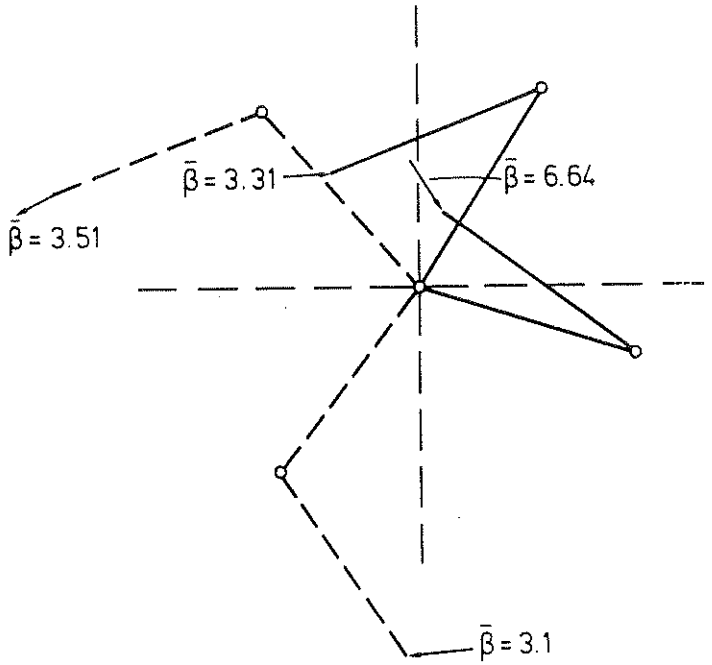

Fig. 8 Load–space configurations for various load levels β for the system with $\gamma = 0.4/9$, $\alpha = 1.0$, $\bar{k} = 0.0$, $\bar{\epsilon} = 0.0$ and $\phi_{10} = \phi_{20} = 0.001$

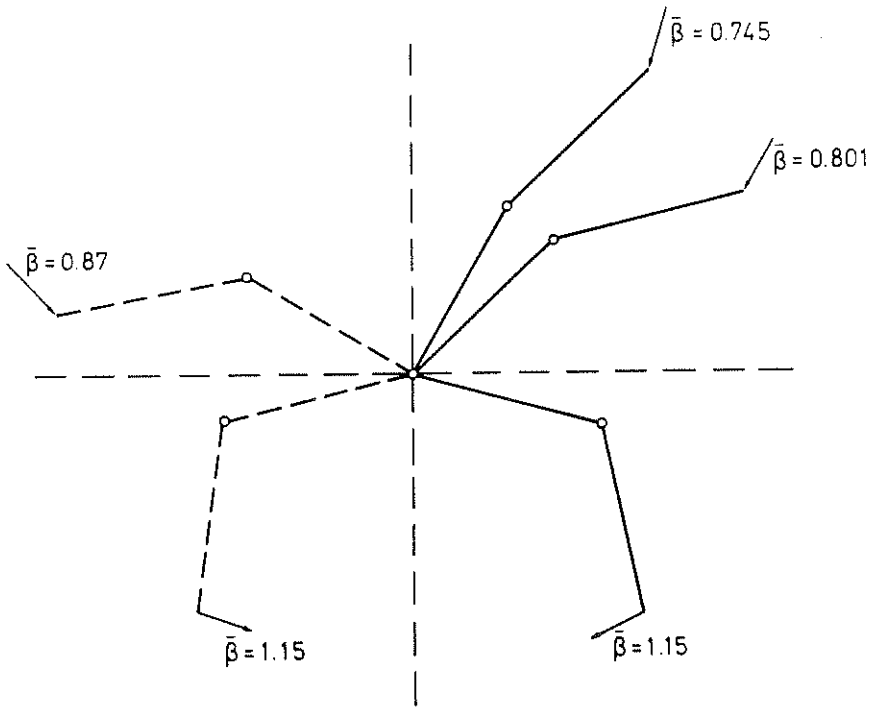

Fig. 9 Configurations for various load levels $\bar{\beta}$ of the model for $\gamma = 0.8$, $\bar{k} = 0.5$, $\bar{\epsilon} = 0.01$ and $\phi_{10} = \phi_{20} = 0.001$

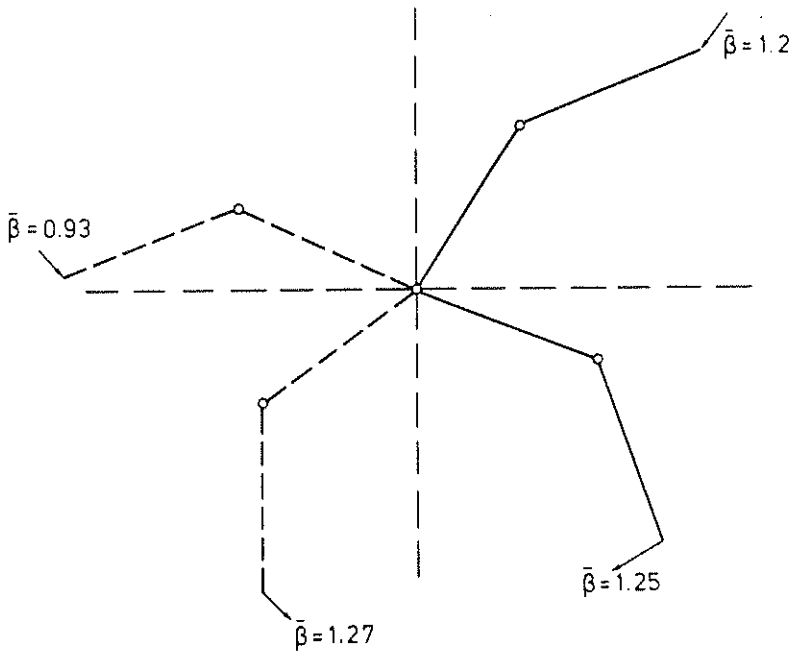

Fig. 10 Configurations for various load levels $\bar{\beta}$ of the model with $\gamma = 0.6$. $\bar{k} = 0.0$, $\bar{\epsilon} = 0.0$, $\alpha = 1.0$ and $\phi_{10} = \phi_{20} = 0.01$

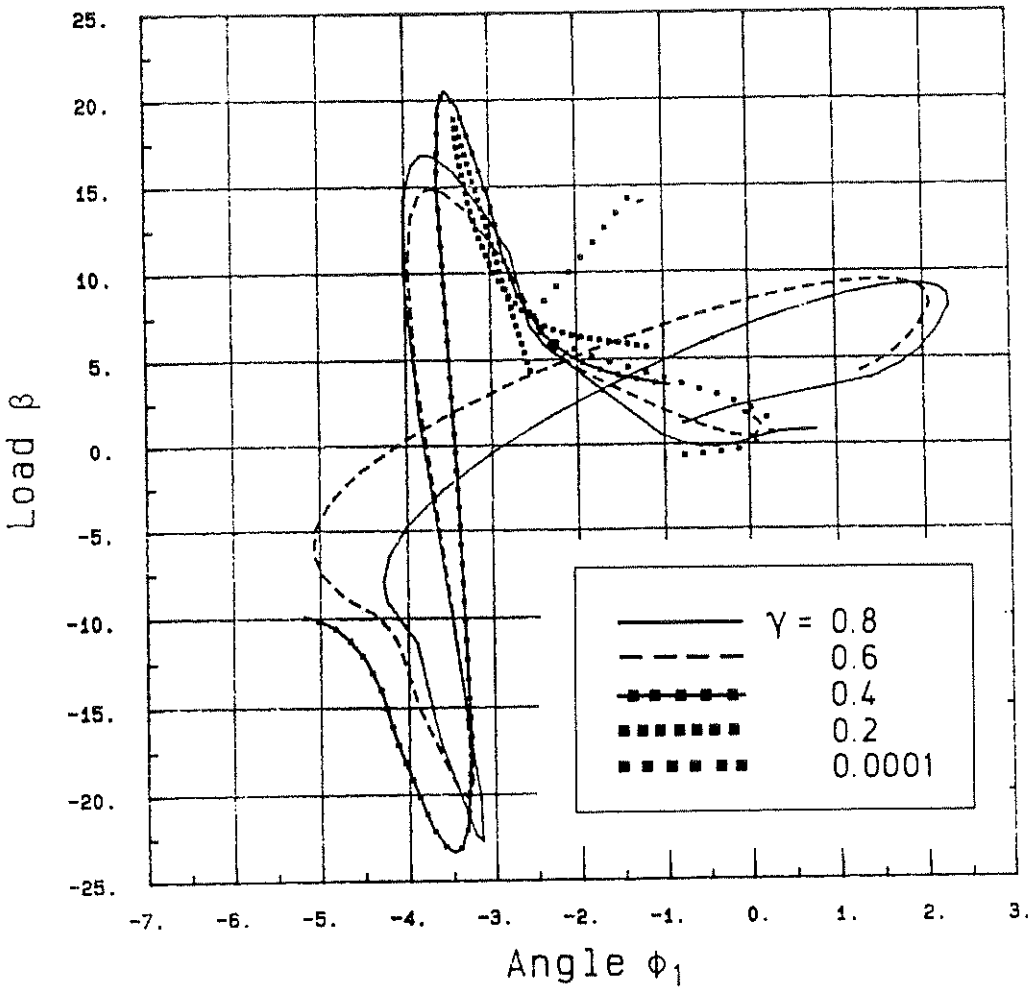

Fig. 11 Loading β versus angle ϕ_1 for five values of the parameter γ and $\bar{k} = 0.5$. $\epsilon = 0.2$, $\alpha = 1.0$, $\phi_{10} = \phi_{20} = 0.001$

1.5 DYNAMIC ANALYSIS OF ONE–DEGREE–OF–FREEDOM SYSTEM

The one–degree–of–freedom mechanical model shown in Figure 1 is reanalyzed dynamically under the assumptions of small deflections.

From d'Alembert's principle we have

$$J\ddot{\phi} + [c - P(1-k-\bar{k})L]\ \phi = Pe \qquad (1.5.1)$$

where J is the moment of inertia of the link about the hinge.

Let

$$\omega_o^2 = \frac{c-P(1-k-\bar{k})L}{J} \tag{1.5.2}$$

where ω_o is the angular frequency

Then equation (1.5.1) becomes

$$\ddot{\phi} + \omega_o^2\phi = \frac{Pe}{J} \tag{1.5.3}$$

Equation (1.5.3) has the following general solution

$$\phi = A_1 \sin\omega_o t + A_2\cos\omega_o t + \frac{Pe}{\omega_o^2 J} \tag{1.5.4}$$

By combining equations (1.5.4) and(1.5.2), an alternative formulae for ϕ is found

$$\phi = A_1\sin\omega_o t + A_2\cos\omega_o t + \frac{Pe}{c-P(1-k-\bar{k})L} \tag{1.5.5}$$

The following initial conditions are stipulated

$$\phi = \dot{\phi} = 0 \quad \text{for} \quad t = 0 \tag{1.5.6}$$

With the above conditions, the constants of integration are found and equation (1.5.5) can be rewritten as

$$\phi = \frac{Pe}{c-P(1-k-\bar{k})L}\ [1-\cos\bar{\omega}_o\tau] \tag{1.5.7}$$

For $\phi = \infty$, $\quad \frac{P_c L}{c} = (1-k-\bar{k})^{-1}$ (1.5.8)

where P_c is the buckling load, and equation (1.5.7) can be written as follows

$$\phi = \frac{\beta\epsilon}{1-\beta/\beta_c}\ (1-\cos\bar{\omega}_o\tau) \tag{1.5.9}$$

with $\beta = PL/c$, $\beta_c = P_cL/c$, $\epsilon = e/L$, $\tau = t\sqrt{c/J}$ and $\bar{\omega}_o^2 = 1 - \beta/\beta_c$ (1.5.10)

Differentiating equation (1.5.9) twice yields

$$\ddot{\phi} = \frac{\beta\epsilon\bar{\omega}_o^2}{1-\beta/\beta_c}\cos\bar{\omega}_o\tau \tag{1.5.11}$$

Substituting for $\bar{\omega}_o^2$ from equation (1.5.10), then for $\tau = 0$ initial angular acceleration will be $\beta\epsilon$. The angular frequency and the static load–angle relations are

$$\bar{\omega}_o = \sqrt{1-\beta/\beta_c} \tag{1.5.12}$$

$$\phi_s = \frac{\beta\epsilon}{1-\beta/\beta_c} \tag{1.5.13}$$

Now the dynamic torsional angle can be rewritten in terms of the static torsional angle

$$\phi_d = \phi_s(1-\cos\bar{\omega}_o\tau) \tag{1.5.14}$$

Equation (1.5.14) describes a system with harmonic oscillation around the static equilibrium position ($\phi_d = \phi_s$) with an amplitude of ϕ_s.

With the increase in the ratio β/β_c, ϕ_s increases and becomes infinite as β/β_c approaches 1.0. The frequency will become zero at that ratio ($\beta/\beta_c = 1.0$).

Equation (1.5.3) have been integrated for various values of the parameters k, $\bar{k}$, ϵ and β/β_c. Figure 12 shows the torsional angle ϕ and its velocity against time $\dot{\phi}$ for an eccentricity of loading $\epsilon = 0.1$. The phase portrait for the same case is shown in Figure 13.

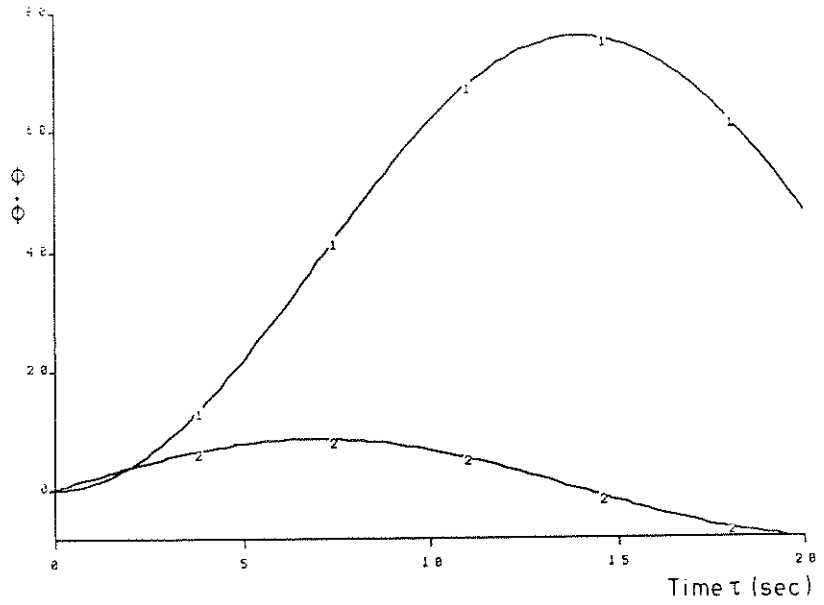

Fig. 12 Time–space–path and velocity–time curve with β =19.0, k = 0.95, ϵ = 0.1 and $\bar{k}$ = 0.0

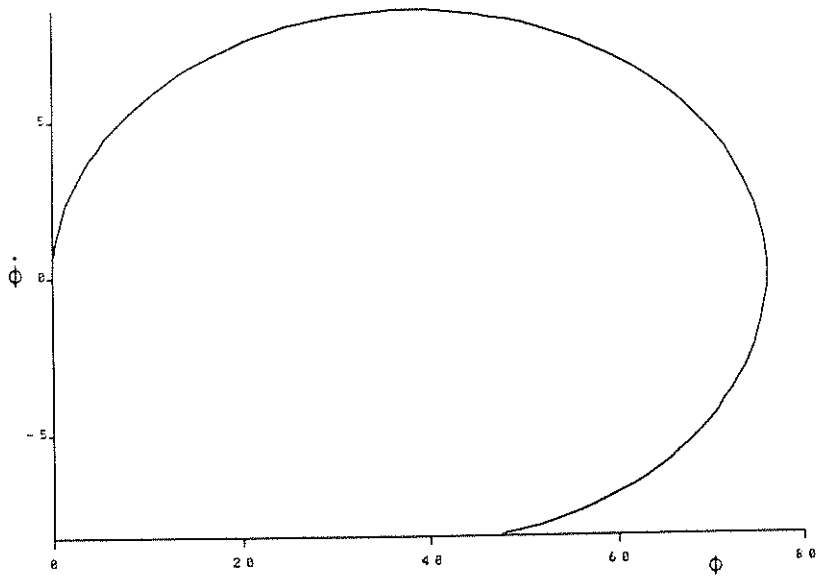

Fig. 13 Phase–portrait ($\dot{\phi}$ – $\dot{\phi}$ relation) for the case shown in Figure 12

1.6 DYNAMIC STABILITY OF AN ELASTOPLASTIC STRUT UNDER A PARTIAL FOLLOWER LOAD

This section deals with the dynamic stability of a damped one–degree–of–freedom strut compressed by a partial follower force at the top. The deformable hinge cell has a bilinear stress–strain relationship. The influence of the tip mass offset and its inertia on the stability is also included.

1.6.1 *Fundamental equations*

Consider a strut, Figure 14, of length L with a partial follower force P at the free end applied with an eccentricity e. The strut is fixed at its lower end to a deformable cell. The elements of the cell have a stress – strain curve as shown in Figure 15. The notations used in this section are:

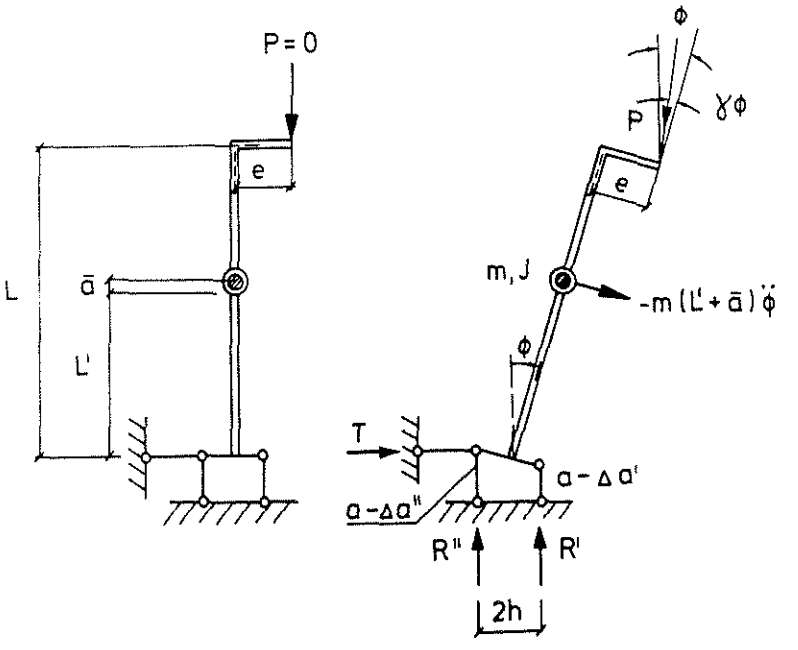

Fig. 14 One–degree–of–freedom model with an elastoplastic hinge cell and loaded by a partial follower force

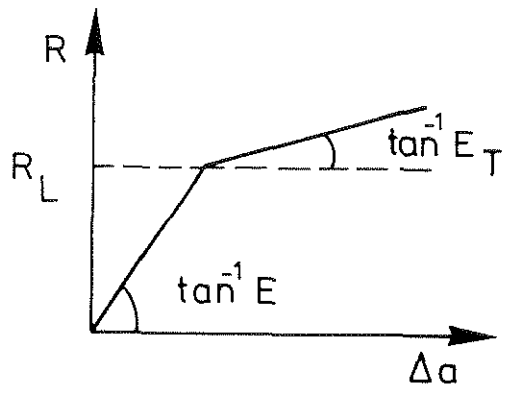

Fig. 15 Stress – strain curve for the deformable hinge cell

b is the damping coefficient

$\bar{a}$ is the concentrated mass's centre of gravity offset

J is moment of inertia of the strut.

Assuming the small displacement range of the angle of rotation ϕ, the equations of equilibrium between the external and internal forces are

$$R' + R'' = P \tag{1.6.1}$$

$$M = PL\gamma\phi - [m(L' + \bar{a})^2 + J]\ddot{\phi} - b\dot{\phi} + Pe = (R' - R'')h \tag{1.6.2}$$

and

$$\Delta a' = \bar{\alpha}h\phi$$
$$\Delta a' - \Delta a'' = 2h\phi$$
$$\Delta a'' = (\bar{\alpha} - 2)h\phi \tag{1.6.3}$$

where $\Delta a'$ and $\Delta a''$ are contractions of the deformable elements of the hinge and 2h is the spacing between them.

Case 1 $P > 2R_L$

Referring to Figures 16a and 16b, then equations (1.6.1) and (1.6.3) yield

$$\bar{\alpha} = \frac{2E}{E+E_T} \tag{1.6.5}$$

hence

$$M = \frac{4EE_T}{E+E_T} h^2\phi = S_k \phi$$

where

$$S_k = \frac{4EE_T}{E+E_T} h^2 \qquad (1.6.6)$$

Case 2 $\quad P < 2R_L$

As $E_T \Rightarrow E$, equation (1.6.5) yields $\bar{\alpha} = 1$
hence

$$M = S\phi \text{ with } S = 2Eh^2 \qquad (1.6.7)$$

Equation (1.6.2) is rewritten, using the following nondimensional quantities

$$q = \frac{PL\gamma}{S} \qquad \bar{\epsilon} = e/\gamma L = \epsilon/\gamma$$

$$c = \bar{a}/L \qquad \mu = mL^2$$

$$\tau = t\sqrt{S/\mu} \qquad \alpha = L'/L$$

$$\beta = \frac{b}{\sqrt{\mu S}} \qquad I_o = \frac{J}{\mu}$$

$$\epsilon = \frac{e}{L} \qquad (1.6.8)$$

$$\frac{M}{S} = q\phi - \ddot{\phi}[(c+\alpha)^2 + I_o] - \beta\dot{\phi} + q\bar{\epsilon} \qquad (1.6.9)$$

Using a generalized moment–angle relationship as in (6c, Reference 28) we have – cf. also equations (1.6.6) and (1.6.7)

$$\frac{M}{S} = k_s(\phi + \bar{\phi}) \qquad (1.6.10)$$

with

$$k_s = \frac{S_k}{S} \text{ for } P > 2R_L \text{ and } k_s = 1 \text{ for } P < 2R_L \qquad (1.6.11)$$

The constant $\bar{\phi}$ is found from the continuity condition of $M - \phi$ at the point of zero velocity.

Assuming the following solution of equation (1.6.9)

$$\phi = A_1 e^{\lambda_1 \tau} + A_2 {}^{\lambda_2 \tau} + \phi^* \tag{1.6.12}$$

then the characteristic equation is

$$\lambda^2 + (\beta/a)\lambda - \left[\frac{q-k_s}{a}\right] = 0 \tag{1.6.13}$$

with

$$a = (c+\alpha)^2 + I_o \tag{1.6.14}$$

The roots of equation (1.6.13) are

$$\lambda_{1,2} = -\frac{\beta}{2a} \pm \sqrt{\left[\frac{\beta}{2a}\right]^2 + \frac{q-k_s}{a}} \tag{1.6.15}$$

1.6.1 Nature of roots

In the absence of damping ($\beta = 0$), the roots of the characteristic equation (1.6.11) are

$$\lambda_{1,2} = \pm \sqrt{\frac{q-k_s}{a}} \text{ for } q > k_s \tag{1.6.16}$$

and

$$\lambda_{1,2} = \pm i \sqrt{\frac{k_s-q}{a}} \text{ for } q < k_s$$

The values of the integration constants A_1 and A_2 are found from the initial conditions

$$\phi = \phi_{10}, \dot{\phi} = \dot{\phi}_{10} \text{ when } \tau = 0.$$

If $q > k_s$
then

$$A_1 = \frac{\dot{\phi}_{10} - \left[\phi_{10} - \phi^*\right]\lambda_2}{\lambda_1 - \lambda_2} \tag{1.6.17}$$

$$A_2 = \frac{-\dot{\phi}_{10} + [\phi_{10} - \phi^*]\lambda_1}{\lambda_1 - \lambda_2}$$

with $\lambda_2 = -\lambda_1$.

$$\text{with} \quad \phi^* = \frac{q\bar{\epsilon} - k_s\,\bar{\phi}}{k_s - q} \tag{1.6.18}$$

For $q < k_s$ and $S_T/S < q < S_k/S$, then the general solution of equations (1.6.9) and (1.6.10) can be written as

$$\phi = \bar{A}_1 \sin\omega\tau + \bar{A}_2 \cos\omega\tau + \phi^* \tag{1.6.19}$$

The integration constants will become

$$\bar{A}_1 = \dot{\phi}_{10}/\omega, \quad \bar{A}_2 = \phi_{10} - \phi^* \tag{1.6.20}$$

where $\omega = \lambda/i$ (1.6.21)

and

$$\phi^* = \frac{[1 - S_k/S] + q\epsilon}{1-q} \tag{1.6.22}$$

For the damped system and in the case of $q < S_k/S$, the roots of equation (1.6.13) will become complex and the general solution of equation (1.6.9) will be

$$\phi = \bar{e}^{\alpha_1 \tau}\ (\bar{\bar{A}}_1 \cos\omega\tau + \bar{\bar{A}}_2 \sin\omega\tau) + \phi^* \tag{1.6.23}$$

where

$$\alpha_1 = -\frac{\beta}{2a}$$

and

$$\omega = \sqrt{\frac{k_s - q}{a} - \left[\frac{\beta}{2a}\right]^2} \tag{1.6.24}$$

The values of the constants $\bar{\bar{A}}_1$ and $\bar{\bar{A}}_2$ with the same initial conditions as in the undamped case are

$$\bar{\bar{A}}_1 = \phi_{10} - \phi^*$$

$$\bar{\bar{A}}_2 = \frac{\dot{\phi}_{10} + \alpha_1(\phi_{10} - \phi^*)}{\omega} \qquad (1.6.25)$$

1.6.2 Numerical calculation

The movements of the strut for various load levels are shown in Figures 16, 17 and 18. Equation (1.6.9) was directly integrated by Runge–Kutta method for various load levels because of the availability of the supporting graphical programs. The initial conditions are $\phi_{10} = 0.1$, $\dot{\phi}_{10} = 0.0$, $S_k/S = 0.2$, $S_T/S = 0.111$, $S = 1.0$ with $\gamma = 1.0$.

For the undamped system without eccentricity and $I_o = \bar{a} = 0.0$, the obtained results are in good agreement with the plotted results of Reference [28], see Figure 19. The damped system with $\beta = 0.01$ is shown in Figure 20. A marked decrease in the value of ϕ is noticed there. For the undamped and eccentric case ($\epsilon = 0.1$) the results are shown in Figure 21. Finally, a damped and eccentric case is studied ($\epsilon = 0.1$, $\beta = 0.01$) and the results are depicted in Figure 22.

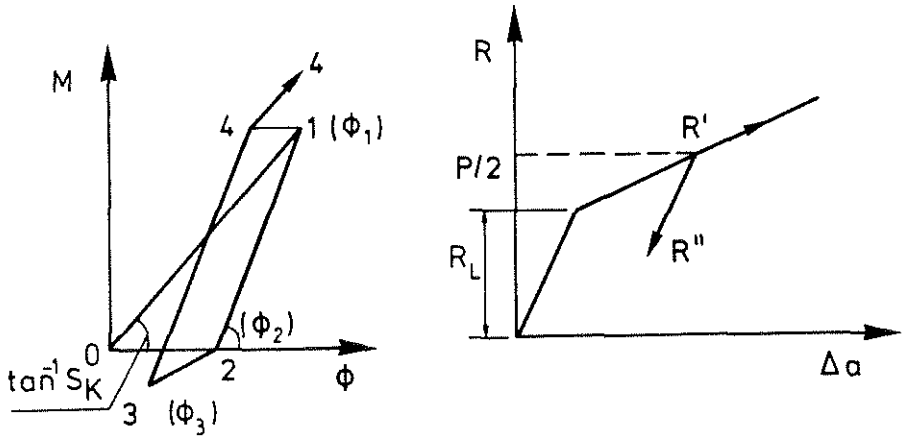

(a) (b)

For $P/2 > R_L$, different positions of the strut

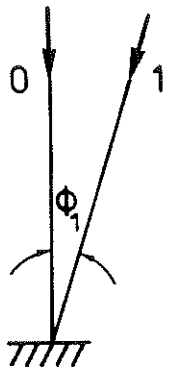

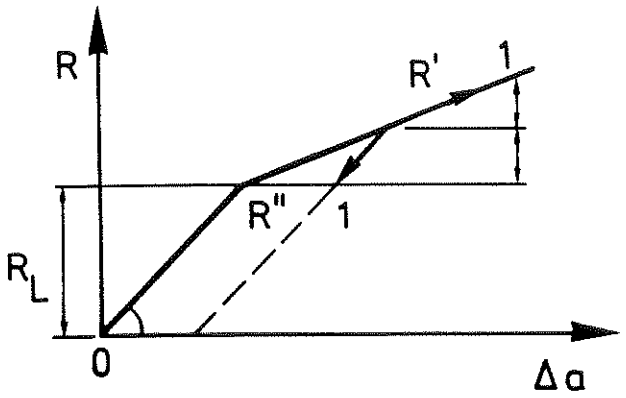

(c) (d)

Strut moves from 0 –1

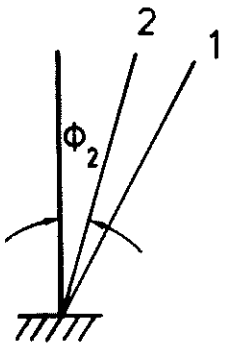

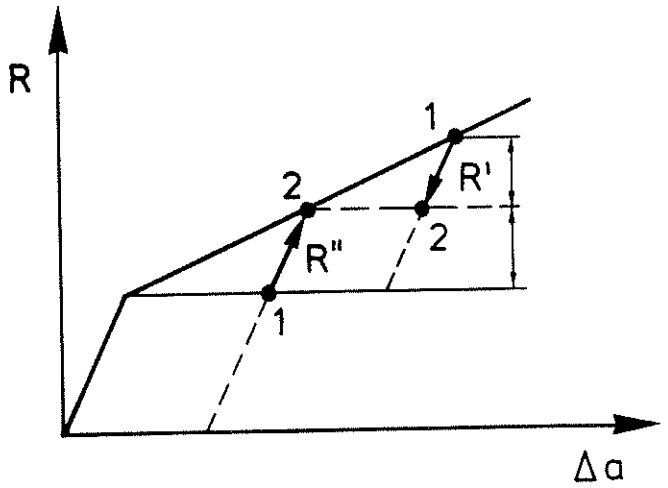

(e) (f)

Strut moves from 1 – 2, R' → P/2, M → 0, $k_S = 1$

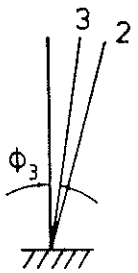

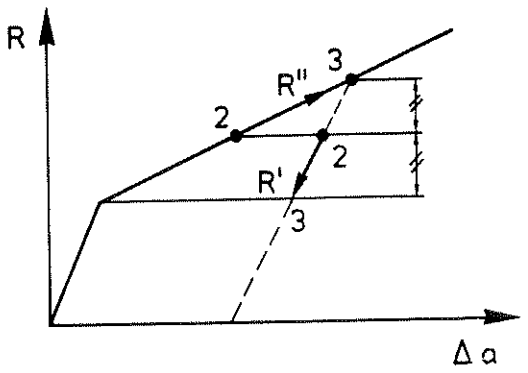

(g) (h)

Strut moves from 2 – 3, $k_S = S_k/S$

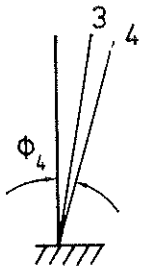

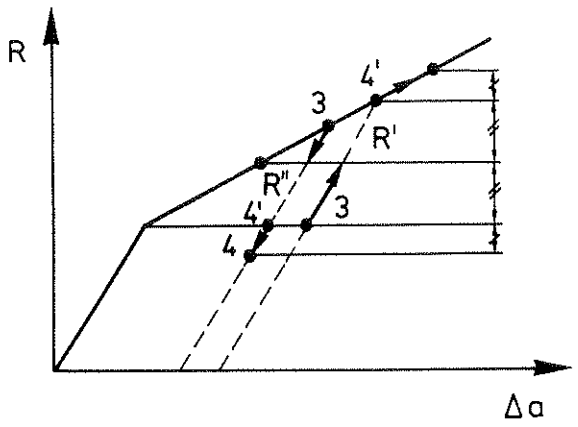

(i) (j)

Strut moves from 3–4 up to point 4', $k_s = 1$ and then $k_s = S_k/S$

Fig.16 (a – j) Moment–angle relationship and force–contraction curves for different positions of the strut when $P/2 > R_L$

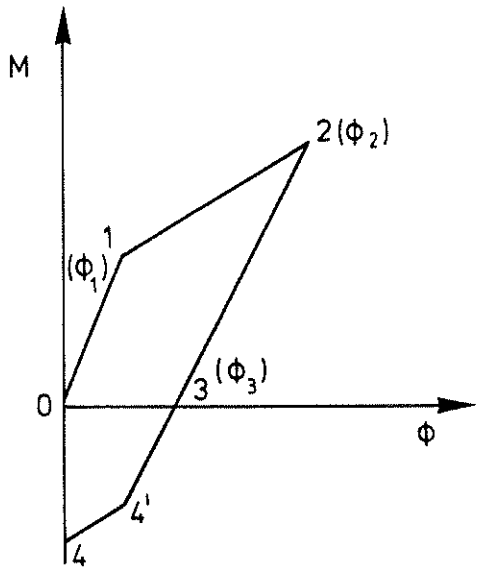

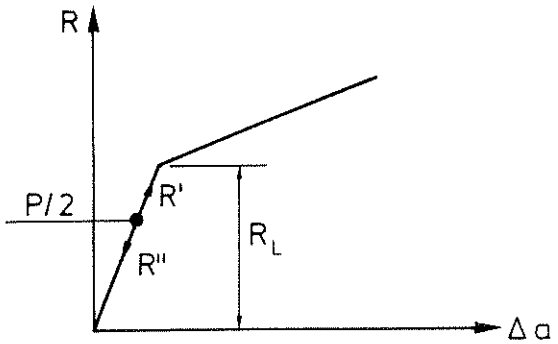

(a) (b)

Fig.17 Moment–angle relationship and force–contraction curve for the strut when $P/2 < R_L$

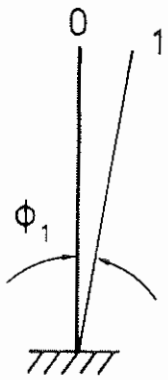

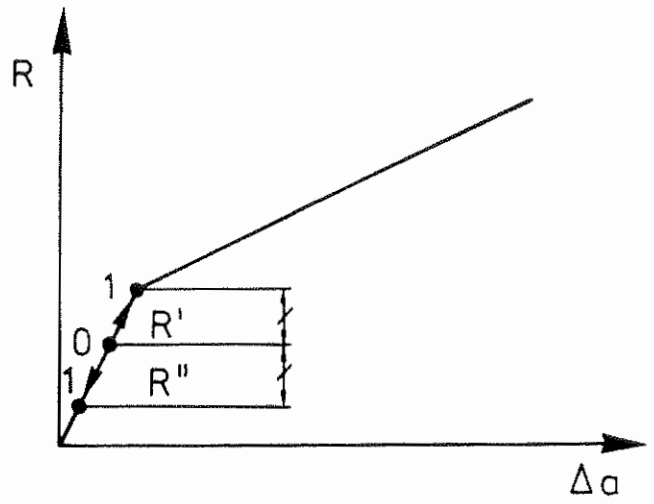

(a) (b)

Strut moves from 0 – 1, $k_s = 1$

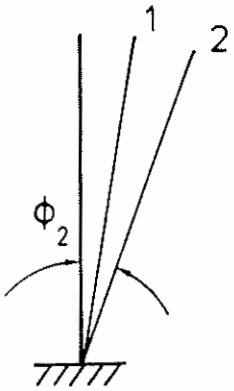

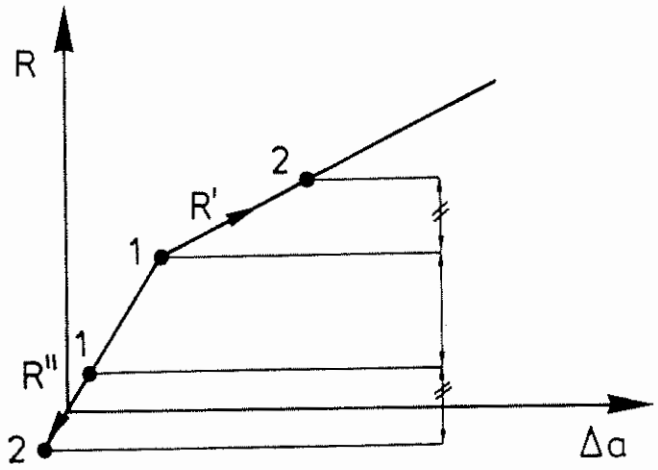

(c) (d)

Strut moves from 1–2, $k_s = S_k/S$

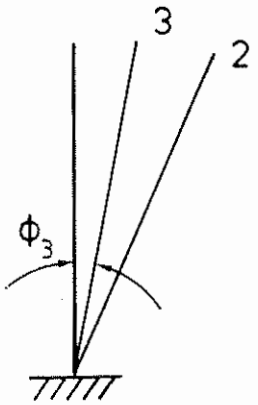

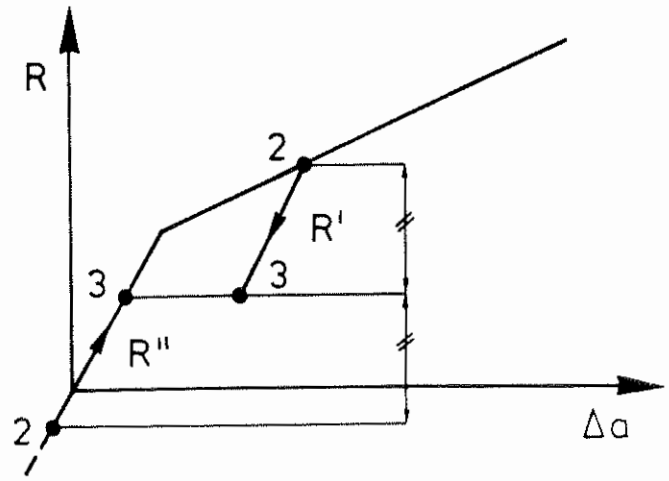

(d) (e)

Strut moves from 2–3, R' → P/2, R" → P/2, M → 0 and $k_s = 1$

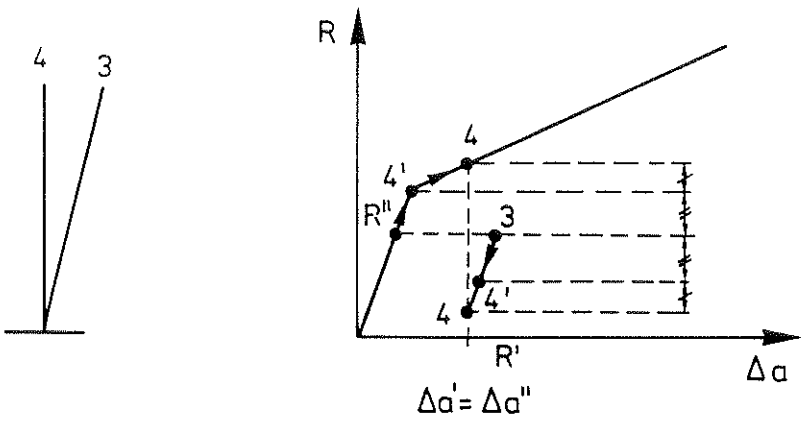

(g) (h)

Strut moves from 3–4, up to point 4' for R'', $k_s = 1$ afterwards $k_s = S_k/S$

Fig. 18 (a – h) Force–contraction curves for different positions of the strut when $P/2 < R_L$

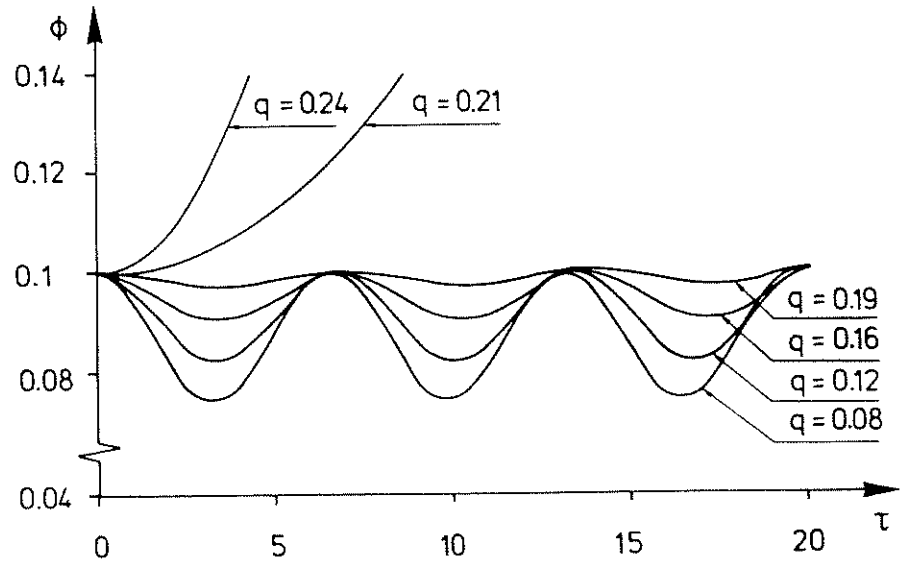

Fig. 19 Time–space paths for undamped system with $\bar{\epsilon} = 0.0$ and $\gamma = 1.0$

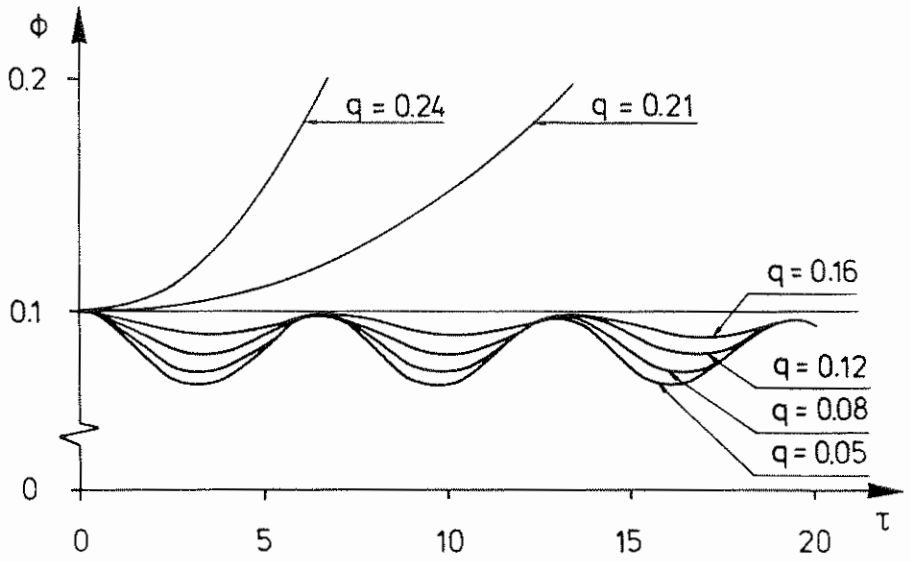

Fig. 20 Time–space paths for the damped system $\beta = 0.01$ with $\bar{\epsilon} = 0.0$ and $\gamma = 1.0$

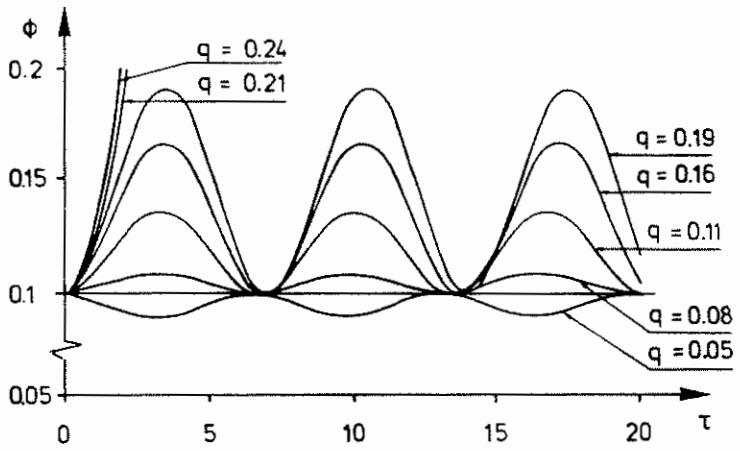

Fig. 21 Time–space paths for the undamped–eccentric system with $\bar{\epsilon} = 0.1$

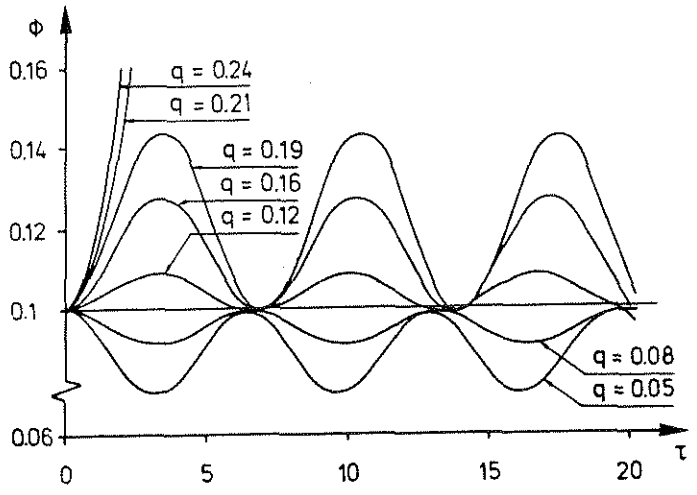

Fig. 22 Time–space paths for the damped system with load eccentricity $\bar{\epsilon} = 0.2$ and $\gamma = 1.0$

1.7 CONTINUOUS SYSTEMS

The simple mechanical models presented in the previous sections are all discrete one– and two–degree–of–freedom idealization of the continuous model shown in Figure 23 and which is dealt with in this section when subjected to an eccentric partial follower force.

1.7.1 Basic equation

The expression governing the static equilibrium configuration is

$$EI\left[\frac{d^2\bar{y}}{dx^2} - \frac{d^2\bar{y}_0}{dx^2}\right] = L\left[\bar{y}_L - \bar{y}\right] - P\phi_p(L - x) + Pe \qquad (1.7.1)$$

Introducing the following quantities

$$\beta = q^2 = \frac{PL^2}{EI},\ \phi_p = k\bar{y}'_L + \bar{k}y_L,\ \epsilon = e/L,\ y = \frac{\bar{y}}{L},\ \xi = x/L \qquad (1.7.2)$$

and

$$f = \frac{\bar{y}_L}{L}$$

Equation (1.7.1) now can be restated in dimensionless form as

$$y'' + q^2 y = q^2[f - (k y'_L + \bar{k} f)(1 - \xi) + \epsilon] + y''_0 \qquad (1.7.3)$$

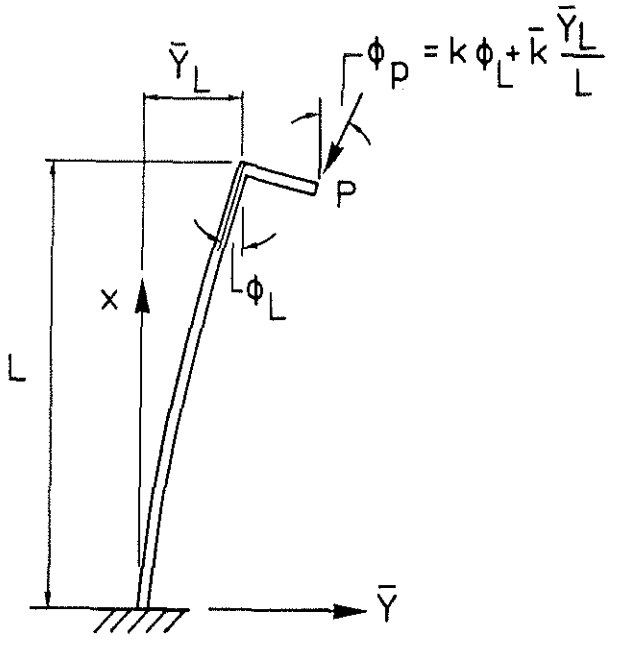

Fig. 23 Cantilever column, compressed by an eccentric follower load

The following boundary conditions are prescribed

$$y(0) = 0 \qquad y'(0) = 0$$
$$y(1) = f \qquad y'(1) = y'_L \qquad (1.7.4)$$

1.7.2 Initial deflection in the form of a cosine function

Assuming an initial deflection in the form

$$y_o = f_o\left[1 - \cos\frac{\pi\xi}{2}\right] \tag{1.7.5}$$

and substituting (1.7.5) into (1.7.3), yields

$$y'' + q^2y = q^2\left[f - (ky'_L + \bar{k}f)(1-\xi) + \epsilon\right] + f_o\frac{\pi^2}{4}\cos\frac{\pi\xi}{2} \tag{1.7.6}$$

The general solution of equation (1.7.6) is

$$y(\xi) = C_1 \sin q\xi + C_2 \cos q\xi + f - (ky'_L + \bar{k}f)(1-\xi) + \epsilon - A\cos\frac{\pi\xi}{2} \tag{1.7.7}$$

with $A = \dfrac{f_o}{1-P/P_e}$, and $P_e = \dfrac{\pi^2 EI}{4L^2}$ (1.7.8)

From the four boundary equations, the following matrix equation is obtained

$$\begin{vmatrix} 0.0 & 1.0 & 1-\bar{k} & -k \\ q & 0.0 & \bar{k} & k \\ \sin q & \cos q & 0.0 & 0.0 \\ q\cos q & -q\sin q & \bar{k} & k-1 \end{vmatrix} \begin{vmatrix} C_1 \\ C_2 \\ f \\ y'_L \end{vmatrix} = \begin{vmatrix} A - \epsilon \\ 0 \\ -\epsilon \\ -A\pi/2 \end{vmatrix} \tag{1.7.9}$$

The matrix equation was solved numerically using subroutines from CALFEM program.

In Figure 24, the deflection of the cantilever under various loads is shown for $k = 0.8$ and $\bar{k} = 0.0$. In Figure 25 the deflected shapes of the cantilever is shown with an eccentricity $\epsilon = 0.05$, $\bar{k} = 00$ and $k = 0.8$.

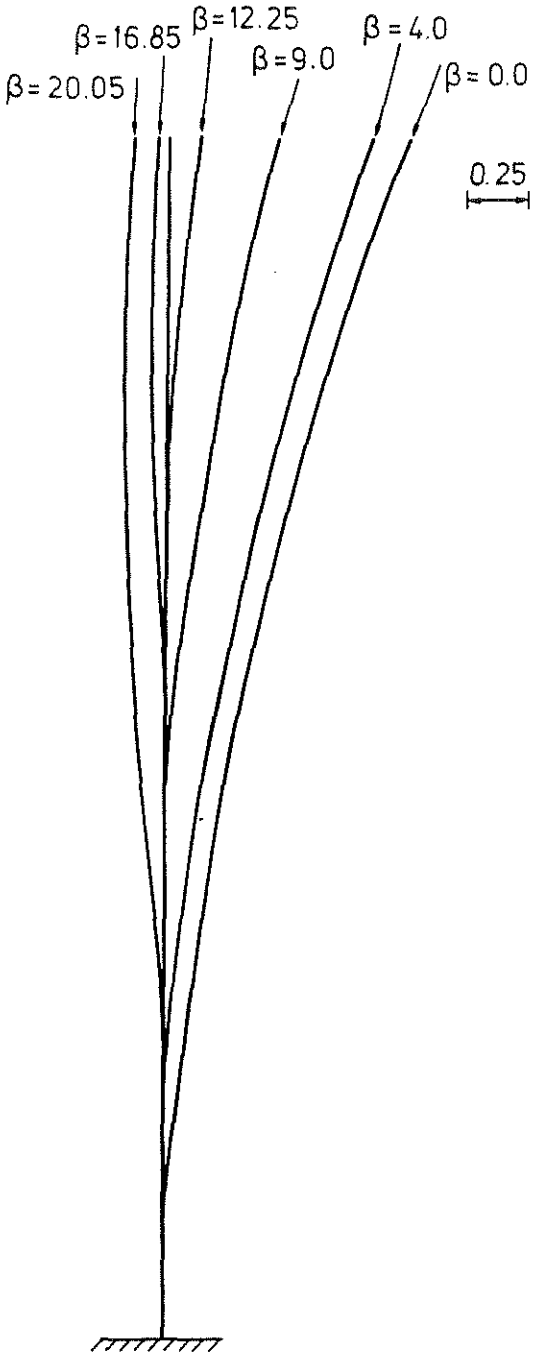

Fig. 24 Deflected forms of the cantilever column with initial curvature in the form

$y_o = f_o\left[1 - \cos\frac{\pi\xi}{2}\right]$, $k = 0.8$, $\bar{k} = 0.0$, $\epsilon = 0$, $L = 20$ cm, $f_o = 1.0$

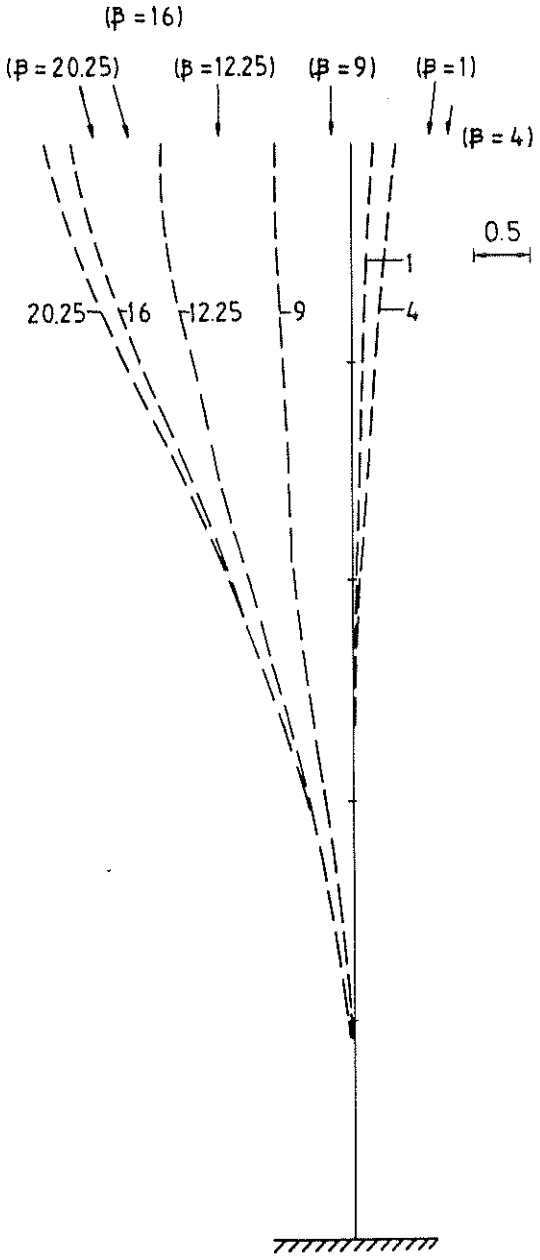

Fig.25 Deflected forms of the cantilever column with an eccentric follower force, k = 0.8, $\bar{k}$ = 0.0, L = 20 cm, e = 1 cm

1.7.3 Initial deflection in the form of the first and second mode shapes of vibration of a cantilever column

The cantilever column in the previous section is reanalysed taking the initial deflection in the form of the first and the second vibration mode shapes of the cantilever. The initial deflection is then expressed as follows

$$y_o(\xi) = f_o[\cos\lambda_i\xi - ch\lambda_i\xi + \tau(\sin\lambda_i\xi - sh\lambda_i\xi)] \tag{1.7.10}$$

Substituting into equation (1.7.3) for $y_o(\xi)$ yields

$$y'' + q^2y = q^2\left\{f - (k\phi_L + \bar{K}f)(1 - \xi) + \epsilon\right\} - f_o\lambda_i^2[\cos\lambda_i\xi + ch\lambda_i\xi + \tau(\sin\lambda_i\xi + sh\lambda_i\xi)] \tag{1.7.11}$$

The values of the constants λ_i and τ are given in table 1.

mode of vibration	λ_i	τ
first mode	1.875	–0.734
second mode	4.694	–1.0185

Table 1 Values of λ_i and τ

The general solution of equation (1.7.11) is

$$y(\xi) = C_1 \sin q\xi + C_2 \cos q\xi + f - (k\phi_L + \bar{K} f)(1 - \xi) + \epsilon + f_o\left[\frac{\cos\lambda_i\xi + \tau \sin\lambda_i\xi}{1 - q^2/\lambda_i^2} - \frac{ch\lambda_i\xi + \tau\, sh\lambda_i\xi}{1 + q^2/\lambda_i^2}\right] \tag{1.7.12}$$

Let $q^2/\lambda_i^2 = s$ (1.7.13)

From the boundary equations (1.7.4), the following matrix equation is obtained

$$\begin{vmatrix} 0.0 & 1.0 & 1-\bar{k} & -k \\ q & 0.0 & \bar{k} & k \\ \sin q & \cos q & 0.0 & 0.0 \\ q\cos q & -q\sin q & \bar{k} & k-1 \end{vmatrix} \begin{vmatrix} C_1 \\ C_2 \\ f \\ \phi_L \end{vmatrix} = \begin{vmatrix} -2f_o s/(1-s^2) - \epsilon \\ -2f_o \lambda_i \tau s/(1-s^2) \\ -f_o V_1 - \epsilon \\ -f_o \lambda_i V_2 \end{vmatrix}$$

where

$$V_1 = \frac{\cos\lambda_i + \tau\sin\lambda_i}{1-s} - \frac{\mathrm{ch}\lambda_i + \tau\,\mathrm{sh}\lambda_i}{1+s} \qquad (1.7.14)$$

$$V_2 = \frac{-\sin\lambda_i + \tau\cos\lambda_i}{1-s} - \frac{\mathrm{sh}\lambda_i + \tau\,\mathrm{ch}\lambda_i}{1+s} \qquad (1.7.15)$$

The constants C_1, C_2, f and ϕ_L are found by a CALFEM subroutine, and examples of the mode shapes of the column are shown in Figures 26.a and b for the first mode of initial deflection with k = 1.0 and for the second mode with k = 1.0.

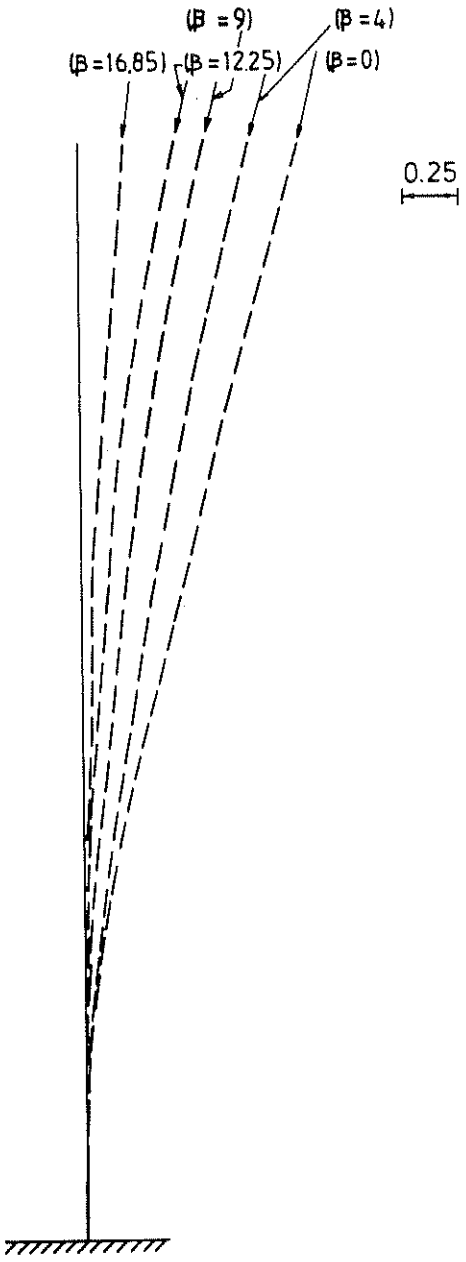

Fig. 26 a Deflected forms of the cantilever column with an initial curvature in the form

$y_o = f_o[\cos 1.875\xi - \mathrm{ch}1.875\xi - 0.734(\sin 1.875\xi - \mathrm{sh}1.875\xi)]$,

$\bar{k} = 0.0,\ k = 1.0,\ \epsilon = 0,\ L = 20,\ f_o = 0.5$

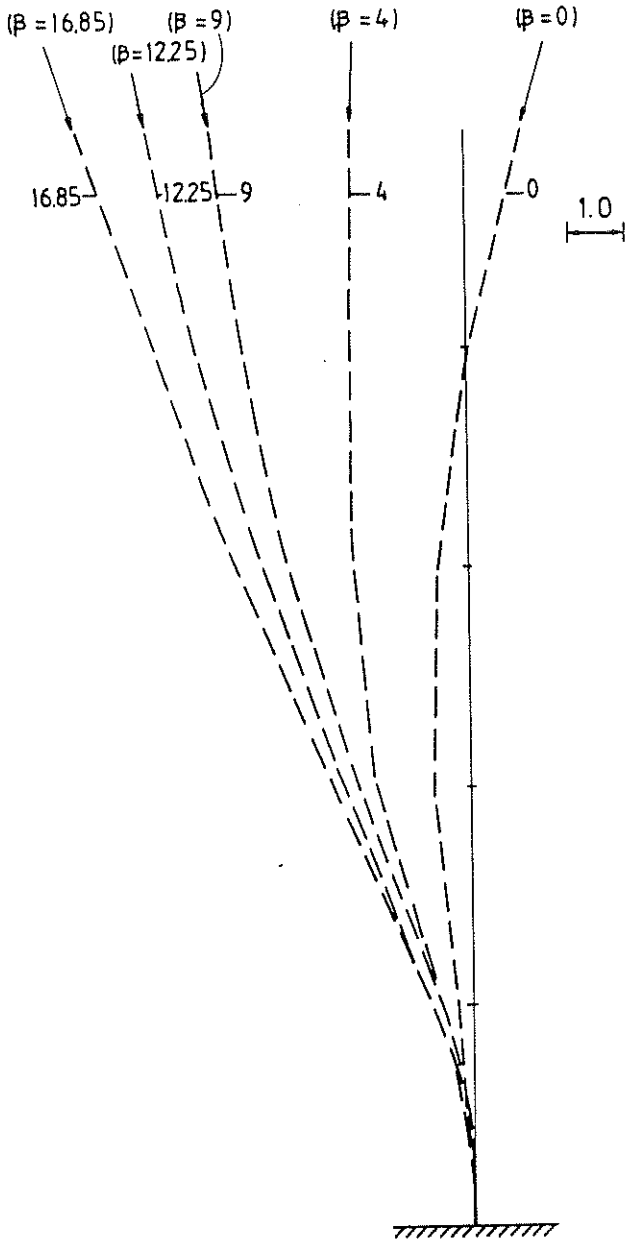

Fig. 26 b Deflected forms of the cantilever column with an initial curvature in the form
$y_o = f_o[\cos 4.694\xi - \mathrm{ch}4.694\xi - 1.018(\sin 4.694\xi - \mathrm{sh}\ 4.694\xi)]$, $k = 0.8$, $\bar{k} = 0$, $\epsilon = 0$, $L = 20$ cm, $f_o = 0.5$

1.8 INSTABILITY OF SPACECRAFT BOOMS DUE TO THERMAL–RADIATION

Thermally exited flexural vibrations of booms have been observed and described in the literature [27, 42]. Flutters of struts subjected to radiant heat has been investigated by Augusti [27]. He used a Rider–Ziegler model of one– and two––degree–of–freedoms.

In this section, a continuous cantilever column, shown in Figure 27, is studied. The results obtained are a generalization of Augusti's paper [43].

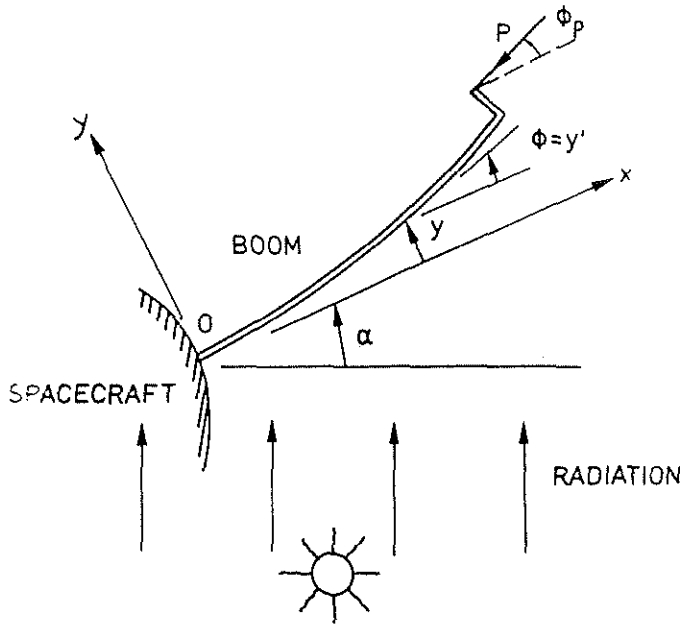

Fig. 27 Spacecraft boom

The radiation equation is given as in Reference [27]:

$$\gamma = \alpha_t^* ka/Hh = k_1 a/H \tag{1.8.1}$$

For pure bending, the thermal curvature is related to the heat input per unit length of the boom, however it lags by a characteristic time τ. The differential equation governing the thermal curvature k_t as proposed by Etkin and Hughes [45] and reported by Yu [42] can be written as

$$\omega\left[\frac{\partial k_t}{\partial \alpha}\right] + k_t/\tau = k_o \cos(\alpha + \phi) \tag{1.8.2}$$

The truncated solution of equation (1.8.2) is

$$k_t = (k_1/H)\ \cos\alpha - (k_1/H)\ \sin(y'-\tau\dot{y}') \tag{1.8.3}$$

where k_1 and k^* are non–negative thermal constants with

$$H = 1/\tau \tag{1.8.3.a}$$

For small values of ϕ, the phase lag of the thermal bending from reference [45] is given by

$$\alpha_o = \tan^{-1}(\omega\tau) \tag{1.8.3.b}$$

ω is the satellite spin rate and α defines the boom attitude. The characteristic time depends on the geometrical construction of the boom and the thermal conductivity of the materials of the boom.

The static equilibrium equation (1.7.3) of section 1.7 is modified to include the effect of thermal bending and becomes, if initial deflection y_o is excluded

$$y'' + q^2y - 2\gamma_1y' = -2\gamma_1\ \cot\alpha + q^2(\epsilon + f) - q^2(k\phi_L + \bar{k}f)\ (1-\xi)$$

where

$$\gamma_1 = (-k_1L/2H)\ \sin\alpha \tag{1.8.4}$$

The general solution of the above equation is

$$y = C_1e^{\lambda_1\xi} + C_2e^{\lambda_2\xi} + \epsilon + f - (k\phi_L + \bar{k}f)\left[1 - \xi - \frac{2\gamma_1}{q^2}\right] - \frac{2\gamma_1}{q^2}\ \cot\alpha \tag{1.8.5}$$

The following boundary conditons are stipulated

$$y(0) = y'(0) = 0$$
$$y(1) = f, \quad y'(1) = \phi_L \tag{1.8.6}$$

From the boundary equations, the constants of integration can be found pending on the roots of the following equation

$$\lambda^2 + q^2 - 2\gamma_1\lambda = 0 \tag{1.8.7}$$

Now the roots are

$$\lambda_{1,2} = \gamma_1 \pm U \text{ and } U = (\gamma_1^2 - q^2)^{1/2} \tag{1.8.8}$$

For real and different roots the following matrix equation must be solved

$$\begin{vmatrix} 1 & 1 & 1-\bar{k}(1-m) & k(m-1) \\ \lambda_1 & \lambda_2 & \bar{k} & k \\ e^{\lambda_1} & e^{\lambda_2} & \bar{k}m & km \\ \lambda_1 e^{\lambda_1} & \lambda_2 e^{\lambda_2} & \bar{k} & k-1 \end{vmatrix} \begin{vmatrix} C_1 \\ C_2 \\ f \\ \phi_L \end{vmatrix} = \begin{vmatrix} n-\epsilon \\ 0 \\ n-\epsilon \\ 0 \end{vmatrix}$$

with

$$m = 2\gamma_1/q^2, \; n = m\cot\alpha \tag{1.8.9}$$

To find the stability boundaries of the system, equation (1.8.4) is differentiated twice and the boundary equations are restated thus

$$y^{IV} + q^2y'' - 2\gamma_1y''' = 0 \tag{1.8.10}$$

$$y(0) = y'(0) = 0 \quad \text{for } \xi = 0$$

$$y''(1) - k_t(1) = 0 \quad \text{for } \xi = 1$$

$$y''(1) - k_t'(1) = -q^2[(1 - k)y' - \bar{k}y] \tag{1.8.11}$$

Using equations (1.8.10) and (1.8.11) and after some algebra, a stability determinant is obtained. In Figure 28 the critical loading ($\beta = q^2$) versus γ_1, is shown, for four values of the nonconservativeness parameter k. The values for $k = 0$ coincides with the values obtained by Augusti.

The regions of dynamic instability and divergence are marked with $S = ib$ and $S = 0$, respectively, as in Reference [43].

Augusti in Reference [27] concludes that for the undamped system, the small oscillation of the boom pointing into the half space away from the radiant heat source will be fanned by the heat source. The heat absorbtion in Augusti's case

depends on the angle with respect to the boom. Figure 29 and 30 show the deflections of the boom compressed by a centric and an eccentric follower force ($\epsilon = 0.1$).

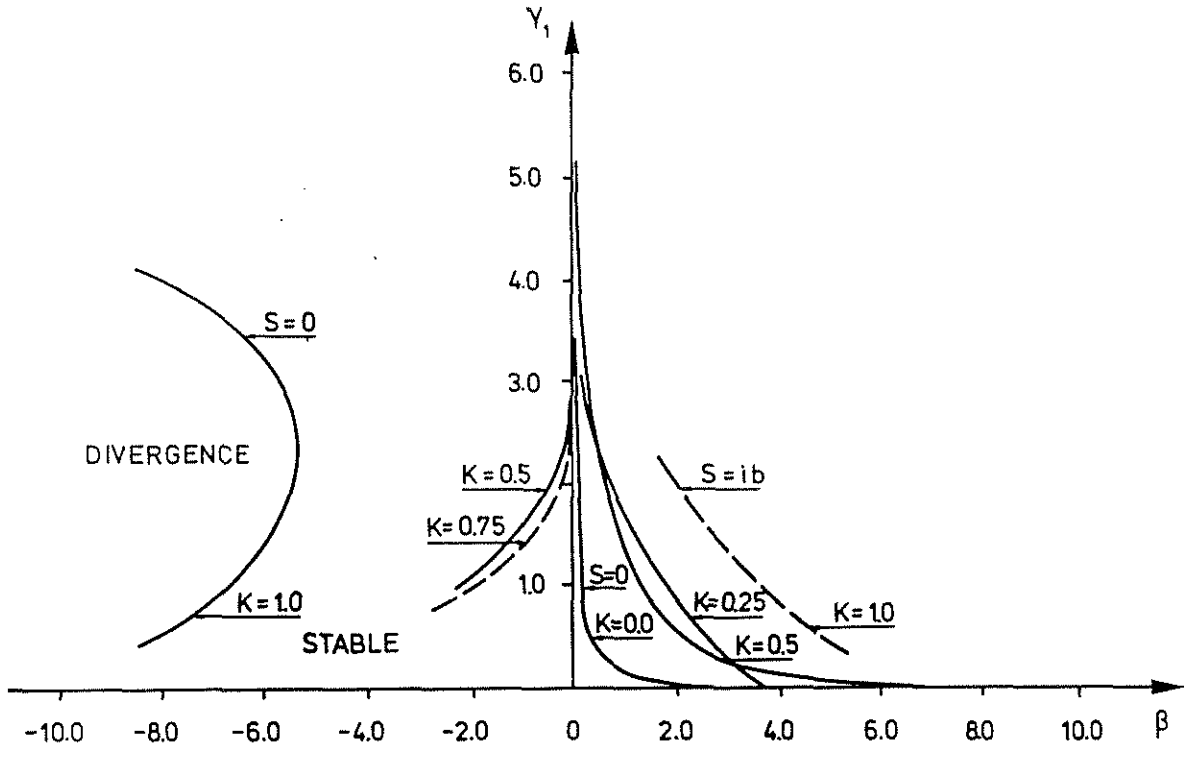

Fig. 28 Critical loading β versus the parameter γ_1, for various values of the nonconservative parameter k

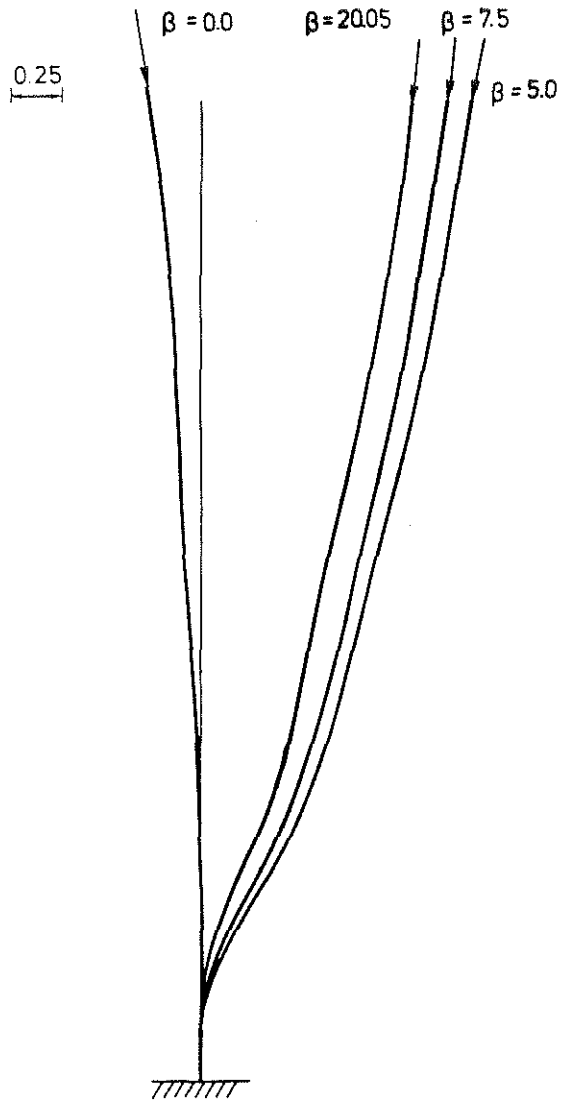

Fig. 29 Deflected shapes of the strut subjected to a centric follower force and thermal radiation with $\epsilon = 0.0$, k = 1.0, $\gamma_1 = 1.1$, $\alpha = 85^0$, L = 20 cm

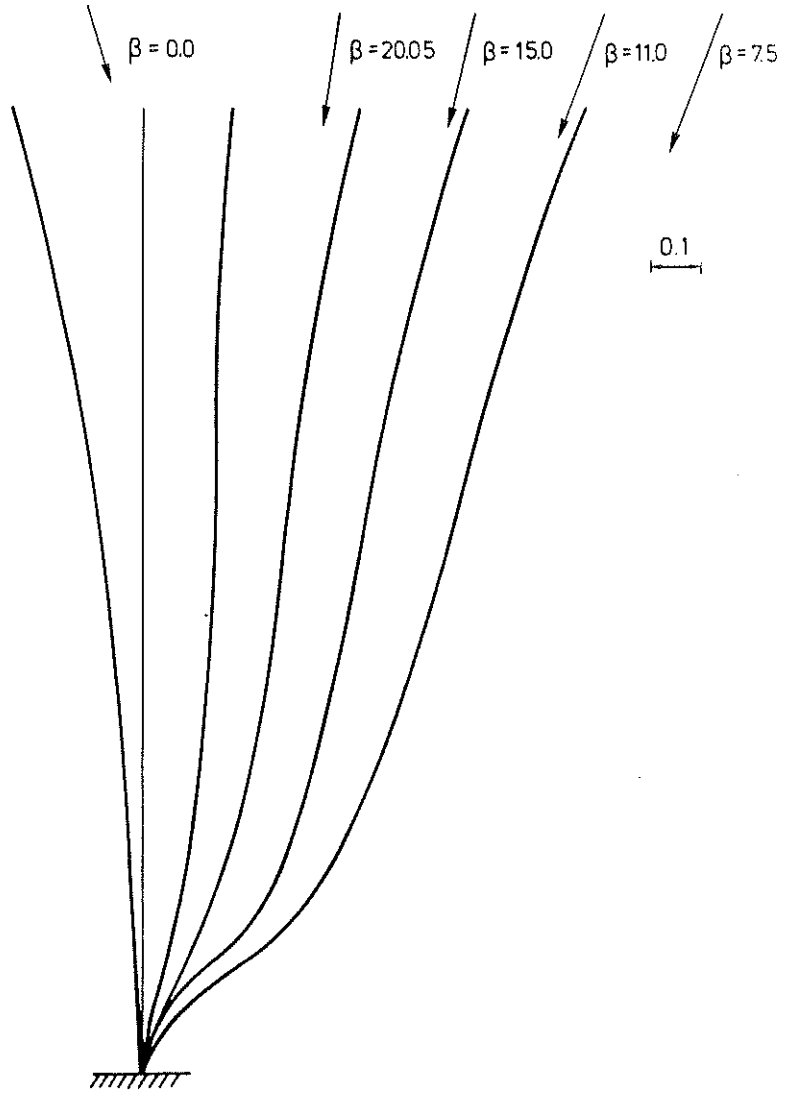

Fig. 30 Deflected shapes of the strut subjected to an eccentric follower force and thermal radiation with k = 1.0, γ_1 = 1.1, α = 85^0, L = 20 cm, ϵ = 0.5

NOTATIONS

L, L_1, L_2	lengths of the rigid links
c	stiffness at the lower and upper hinges, respectively
ϕ_{10}, ϕ_{20}	initial out–of–plumb of the upright of the links, respectively
ϕ_1, ϕ_2	configuration angles from the vertical
ϕ_p	the angle from the vertical at which the follower force acts with respect to the upper end of the link or the upper link
P	follower force acting at the end of column or at the end of upper link
k, $\bar{k}$, γ	nonconservative parameters
e	eccentricity
J	moment of inertia of the link about the lower hinge
ω_o	angular frequency
t, τ	time or dimensionless time
b	damping coefficient
$\bar{a}$	concentrated mass's centre of gravity offset
m	mass of the concentrated mass
E	elastic modulus
E_T	tangent modulus

S, S_T, S_k	elastic modulus, Shanley modulus and von Kármán modulus, respectively
$\bar{\omega}_o$	dimensionless frequency
k_s	elasto–plastic spring modulus
α	dimensionless length
β	dimensionless load
β_c	critical buckling load
f_o	initial curvature constant in section 1.7.3
x	axial coordinate
y	lateral displacement of the column
y_o	initial value of y with no load
γ	measure of radiation intensity
τ	Yu's characteristic time
H	emission parameter in Augusti model
a	length of the lumped thermal cell in Augusti model
k^*, k_1	non–negative constants in Augusti model
α_t	coefficient of thermal expansion
h	depth of the cell
k_o	thermal bending constant

k_t thermal curvature

ω satellite spin rate

α_o phase lag of the thermal bending

α boom attitude

REFERENCES

[1] Bolotin, V.V., Nonconservative Problems of the Theory of Elastic Stability, the Macmillan Co., New York, N.Y., 1963

[2] York, D.L., Structural Behaviour of Driven Piling, Highway Research Record, No.333, pp.60–72, 1971

[3] Burgess, I.W., A Note on the Directional Stability of Driven Piles, Geotechnique, Vol.25, No.2, pp.413–416, 1975

[4] Burgess, I.W. and Tang, C.A., Effect of Driving Support Conditions on Pile Wandering, Institution of Civil Engineers, pp.9–17, 1980

[5] Horikawa, H., Active Feedback Control of an Elastic Body Subjected to Nonconservative Force, Ph.D. Thesis, Princeton University, July 1977

[6] Claudon, J., Optimal Stability of Distributed Structures Governed by Non–self–adjoint, Multi–parameter Eigenvalue Problems, Ph.D. Thesis, Tokyo University, June 1981

[7] Sugiyawa, T., Kashima K. and Kawagoe, H., On an Unduly Simplified Model in the Nonconservative Problems of Elastic Stability, J. Sound and Vibrations, Vol 45, pp.237/247, 1976

[8] Koiter, W.T., *On the Stability of Elastic Equilibrium*, Ph.D. Thesis, Delft. 1945, English Translation, NASA, TT, F10, 833, 1967

[9] Sewell, M.J., The Static Perturbation Technique in Buckling Problems, J. Mech. Phys. Solids, Vol.13, pp.247–265, 1965

[10] Thompson, J.M.T. and Hunt, G.W., A General Theory of Elastic Stability. John Wiley & Sons, New York, 1974

[11] Huseyin, K., Elastic Stability of Structures Under Combined Loading, Ph.D. Thesis, University College, London University, 1967

[12] Burgess, I.W. and Levinson, M., The Post–Flutter Oscillations of Discrete Symmetric Structural Systems With Circulatory Loading, Int. J. Mech. Sci. 14, pp.471–488, 1972

[13] Plaut, R.H., Post–Buckling Behaviour of a Double Pendulum With Partial Follower Load, Report No VPI–E–76–2, Virginia Polytech. Institute and State University, Blacksbury, Virginia, February 1976

[14] Plaut, R.H., Branching Analysis at Coincident Buckling Loads of Non–Conservative Elastic Systems, Report No VPI–E–76–15, Virginia Polytechnic Institute and State University, Blacksbury, Virginia, August 1976

[15] Plaut, R.H., Post–Buckling Behaviour of Continuous, Nonconservative Elastic Systems, Acta Mechanica 30, pp.51–64, 1978

[16] Hagedorn, P., On the Destabilizing Effect of Non–Linear Damping in Non–conservative Systems with Follower Forces, Int. J. Non–Linear Mechanics, Vol.15, June 1970

[17] Sethna, P.R. and Shapiro, S.M., Nonlinear Behaviour of Flutter Unstable Dynamical Systems With Gyroscopic and Circulatory Forces, J. Appl. Mech. 44, pp.755–762, Dec 1977

[18] Guckenheimer, J. and Holmes, P., Nonlinear Oscillations, Dynamical Systems and Bifurcations to Vector Fields, Springer–Verlag, 1983

[19] Scheidl, R., Troger, H. and Zeman, K., Coupled Flutter and Divergence Bifurcation of A Double Pendulum, Int. J. Non–Linear Mech., Vol.19, No 2, pp.163–176, 1983

[20] Jin, J.D. and Matsuzaki, Y., Bifurcations in a Two–Degree–of–Freedom Elastic System with Follower Forces, J. Sound and Vibration, Vol.126, pp.265–277, 1988

[21] Kounadis, A.N., New Instability Aspects for Nonlinear Nonconservative Systems with Precritical Deformation, Nonlinear Dynamics in Engineering Systems, INTAM Symposium Stuttgart/Germany, 1989, Spring–Verlag 1990

[22] Mandadi, V. and Huseyin, K., Non–linear Bifurcation Analysis of Non–Gradient Systems, Inst. J. Non–Linear Mech. Vol.15, pp.159–172, 1980

[23] Bourières, F.J., Sur un Phenomène d'Oscillation Auto–entretenne en Méca–nique de Fluides Réels, Publications Scientifiques et Téchniques du Minis–tère de I'Air, No.147, 1939

[24] Gregory, R.N. and Paidoussis, M.P., Unstable Oscillation of Turbular Can–tilevers Conveying Fluids. Parts I, II, Proceedings of the Royal Society (London), Vol.293, pp.512–542, 1966

[25] Benjamin, B.I., Dynamics of a System of Articulated Pipes Conveying Fluid, Part I & II, Proceedings of the Royal Society (London), Vol.261, pp.457–499, 1961

[26] Mote, C.D. Jr., Dynamic Stability of Axially Moving Materials, Shock and Vibration Digest, Vol.4(4), pp.2–11, 1972

[27] Augusti, G., Instability of Struts Subjected to Radiant Heat, Meccanica Vol.3, pp.167–176, 1968

[28] Augusti, G., Dynamic Analysis of an Inelastic Strut, Giorn. Genio. Civile, Vol.8(103), pp.396–405, 1965

[29] Chernukha, Yu A., Stability of Elastoplastic Pars Compressed by Tangential Force (in Russian), Prikl. Mech, Vol. 5, pp.103–110, 1969

[30] Chernukha, Yu A., Stability of Elastoplsitc Bar Under Tangential Forces (in Russian), Slozhnaya Deformatsia, Tverdova Tele, IZd–Vo, 1969

[31] Kounadis, A.N., Avraam, T.P. and Pantis, M.A., Snap–Through Buckling of a Simple Frame with a Tangential Load, Acta Mechanica 36, pp.119–127, 1980

[32] Kounadis, A.N. and Economou, A.P., The Effects of the Joint Stiffness and of the Constraints on the Type of Instability of a Frame under a Follower Force, Acta Mechanica, Vol.36, pp.157–168, 1980

[33] Kounadis, A.N. and Avraam, T.P., Linear and Nonlinear Analysis of a Nonconservative Frame of Divergence Instability, AIAA Journal 19, pp.761–765, 1981

[34] Argyris, J.H. and Symeonidis, S.P., Nonlinear Finite Element Analysis of Elastic Systems Under Nonconservatiave Loading – Natural Formulation, Comp. Meths. Appl. Mech. Engrg. 26, pp.75–123, 1981

[35] Argyris, J.H. and Symeonidis, S.P., A Sequel to Non–linear Finite Element Analysis of Elastic Systems Under Nonconservative Loading – Natural Formulation, Comp. Meths. Appl. Mech. Engrg. 26, pp.377–383, 1981

[36] Oran, C. and Reagan, R., Buckling of Uniformly Compressed Circular Arches, Journal of the Engineering Mechanics, Trans ASCE EM4, 879–894, 1969

[37] Hasegawa, A., Matsuno, T. and Nishino, F., Planar Buckling and Post––Buckling Behaviour of Rings and Arches Subject to Displacement Dependent Loads, Structural Eng./Earthquake Eng., Vol.6(1), pp.49–57, 1989

[38] Sugiyama, T. and Sekiya, T., Surveys of the Experimental Studies on Instability of the Elastic Systems Subjected to Nonconservative Forces, J Japan Soc. Aero Space Sciences, Vol.19, pp.19–26, 1971

[39] Lundquist, F.E., Strength Tests of Thin–Walled Duralumin Cylinders in Compression, NACA Report No. 493, 1933

[40] Donnel, L.H. and Wan, C.C., Effect of Imperfections of Buckling of Thin Cylinders and Columns Under Axial Compression, J. Appl. Mech. 73, 1950

[41] Pettersson, O., Cirkulatorisk Instabilitet vid Tryckta Strävor och Plattor. Lund Institute of Tech., Dept of Structural Mechanics Publication, 1969

[42] Yu, Y.Y., Reply by Author to P.F. Jordan and G. Augusti and New Results of Two–Mode Approximation Based on a Rigorous Analysis of Thermal Bending Flutter of a Flexible Boom, J. Spacecraft and Rockets, Vol.8, No. 2, pp.205–208, 1971

[43] Augusti, G., Comments on Thermally Induced Vibrations and Flutter of Flexible Booms, J. Spacecraft and Rockets, Vol. 8, No. 1, pp. 77–79, 1971

[44] Augusti, G., Private communication

[45] Etkin, B. and Hughes, P.C., Explanation of the Anomalous Spin Behavior of Satellites with Long, Flexible Antennae, J. Spacecraft and Rockets, Vol. 4, No. 9, pp.1139–1145, Sept. 1967